Journal of Anatomy

J. Anat. (2020) **236**, pp21–49 doi: 10.1111/joa.13084

Virtual endocranial and inner ear endocasts of the Paleocene 'condylarth' *Chriacus*: new insight into the neurosensory system and evolution of early placental mammals

Ornella C. Bertrand[1] Sarah L. Shelley,[2] John R. Wible,[2] Thomas E. Williamson,[3] Luke T. Holbrook,[4] Stephen G.B. Chester,[5,6,7] Ian B. Butler[1] and Stephen L. Brusatte[1,3]

[1] *School of GeoSciences, University of Edinburgh, Grant Institute, Edinburgh, UK*
[2] *Section of Mammals, Carnegie Museum of Natural History, Pittsburgh, PA, USA*
[3] *New Mexico Museum of Natural History and Science, Albuquerque, NM, USA*
[4] *Department of Biological Sciences, Rowan University, Glassboro, NJ, USA*
[5] *Department of Anthropology and Archaeology, Brooklyn College, City University of New York, Brooklyn, NY, USA*
[6] *Department of Anthropology, The Graduate Center, City University of New York, New York, NY, USA*
[7] *New York Consortium in Evolutionary Primatology, New York, NY, USA*

Abstract

The end-Cretaceous mass extinction allowed placental mammals to diversify ecologically and taxonomically as they filled ecological niches once occupied by non-avian dinosaurs and more basal mammals. Little is known, however, about how the neurosensory systems of mammals changed after the extinction, and what role these systems played in mammalian diversification. We here use high-resolution computed tomography (CT) scanning to describe the endocranial and inner ear endocasts of two species, *Chriacus pelvidens* and *Chriacus baldwini*, which belong to a cluster of 'archaic' placental mammals called 'arctocyonid condylarths' that thrived during the *ca*. 10 million years after the extinction (the Paleocene Epoch), but whose relationships to extant placentals are poorly understood. The endocasts provide new insight into the paleobiology of the long-mysterious 'arctocyonids', and suggest that *Chriacus* was an animal with an encephalization quotient (EQ) range of 0.12–0.41, which probably relied more on its sense of smell than vision, because the olfactory bulbs are proportionally large but the neocortex and petrosal lobules are less developed. Agility scores, estimated from the dimensions of the semicircular canals of the inner ear, indicate that *Chriacus* was slow to moderately agile, and its hearing capabilities, estimated from cochlear dimensions, suggest similarities with the extant aardvark. *Chriacus* shares many brain features with other Paleocene mammals, such as a small lissencephalic brain, large olfactory bulbs and small petrosal lobules, which are likely plesiomorphic for Placentalia. The inner ear of *Chriacus* also shares derived characteristics of the elliptical and spherical recesses with extinct species that belong to Euungulata, the extant placental group that includes artiodactyls and perissodactyls. This lends key evidence to the hypothesized close relationship between *Chriacus* and the extant ungulate groups, and demonstrates that neurosensory features can provide important insight into both the paleobiology and relationships of early placental mammals.

Key words: inner ear; brain; 'condylarth'; Euungulata; locomotion; neocortex.

Introduction

Placental mammals are by far the most diverse group of mammals today with 6111 species, compared with marsupials (379 species) and monotremes (five species; Burgin et al., 2018). Placentals, which give live-birth to well-developed young, can be found all around the world in a plethora of ecological niches and display a wide range of body masses (Nowak, 1999). This clade probably started to diversify during the Late Cretaceous when dinosaurs were still the dominant animals on Earth (Murphy et al., 2001; dos Reis et al., 2012, 2014; Liu et al., 2017). The end-Cretaceous cataclysm that killed off non-avian dinosaurs and many other vertebrates about 66 million years ago provided

Correspondence
Ornella C. Bertrand, School of GeoSciences, University of Edinburgh, Grant Institute, Edinburgh, Scotland, UK. E: ornella.bertrand@ed.ac.uk

Accepted for publication *8 August 2019*
Article published online *30 October 2019*

placental mammals with a unique opportunity to thrive (Wible et al., 2007; O'Leary et al., 2013). Some 10 million years into the Paleogene, placental mammals had already displayed a clear increase in taxonomic and ecological diversity, as well as in evolutionary rates, in contrast to their end-Cretaceous relatives (Alroy, 1999; Slater, 2013; Grossnickle & Newham, 2016; Halliday & Goswami, 2016a,b; Halliday et al., 2016). This extrinsic environmental change definitively opened new ecological opportunities for placental mammals; however, intrinsic aspects of placental mammals likely played a role in their success as well (Wilson, 2013).

One of the biological features that may have been integral in the rise of placental mammals is their neurosensory system. Extant mammals have the largest brain relative to body mass of all vertebrates (Jerison, 1973). They have also developed a new region of the forebrain called the neocortex, which integrates sensory and motor information, including high thought process, vision and audition (Jerison, 1973; Martin, 1990). The general neurosensory organization exhibited by extant mammals has been maintained since the Late Triassic-Early Jurassic (e.g. by *ca*. 200 million years ago), when the first mammals and their closest relatives started to emerge (Rowe, 1996; Rowe et al., 2011). Much later, fossils of early members of extant crown placental groups from the Eocene and Oligocene (*ca*. 56–23 million years ago) – including rodents, euprimates and artiodactyls – display neurosensory innovations such as a proportionally larger neocortex, as well as a higher encephalization quotient compared with their Mesozoic ancestors, but not as high as their present-day descendants (Silcox et al., 2009b; Orliac & Gilissen, 2012; Bertrand et al., 2016). However, between these two well-known intervals of mammalian neurosensory evolution, there is a gap: few studies have focused on the brain of the oldest placental mammals living during the early Paleogene, in the Paleocene (66–56 million years ago; Radinsky, 1977; Gingerich & Gunnell, 2005; Silcox et al., 2011; Orliac et al., 2014; Muizon et al., 2015; Napoli et al., 2018; Cameron et al., 2019). This is problematic because these taxa are critical to understanding neurosensory evolution of placental mammals in the aftermath of the end-Cretaceous extinction.

One of the reasons for this gap is that the anatomy and phylogenetic relationships of the placentals living during the first *ca*. 10 million years of the Paleogene remain largely mysterious (Williamson, 1996; Rose, 2006) despite a large diversity of Paleocene placentals – about 690 species known globally from fossils (The Paleobiology Database, 2019). The phylogenetic relationships of these 'archaic' placentals with both their Cretaceous forebears and more recent placentals (including the extant orders) are still unclear (Rose, 2006). This is particularly true for the 'condylarths', a heterogeneous collection of taxa that includes more than 100 species that roamed the Earth during the Paleocene and Eocene. They have been categorized as primitive ungulate-like mammals, and some of them may have given rise to extant perissodactyls and artiodactyls (Prothero et al., 1988; Rose, 2006; O'Leary et al., 2013). However, their classification and relationships are a morass, making 'Condylarthra' one of the most infamous wastebasket groups in paleontology.

Most work on 'condylarths', going back to the studies of Cope (1881a, 1884a,b), Osborn & Earle (1895) and Matthew (1937), used dental and postcranial features to make links to extant placental groups. Recent phylogenetic analyses of these species are dominated by dental characters, which although often highly informative in diagnosing major mammalian clades can also suffer from homoplasy related to dietary convergence and developmental constraints (Kangas et al., 2004; Kassai et al., 2005; Zou & Zhang, 2016; Sansom et al., 2017; Billet & Bardin, 2018). In part this is unavoidable, as teeth make up the vast majority of the fossil record of 'condylarths' and other early placentals. Neurosensory anatomy, however, offers potential for identifying key features that may unite Paleocene 'condylarths' with extant groups, along with helping to understand the behavior of these long-extinct mammals during a time of major ecological, environmental and evolutionary changes. The brains, inner ears and other neurosensory structures of 'condylarths' have been difficult to study because they are not directly preserved in fossils, but the advent of computed tomography (CT) scanning has recently allowed visualization of the internal spaces holding these structures. Thus far, only a few studies have used CT to examine the neurosensory anatomy of 'condylarths' (Orliac & Gilissen, 2012; Orliac et al., 2012a; Ravel & Orliac, 2015; Orliac & O'Leary, 2016; Cameron et al., 2019). More work is thus required to better appreciate the neurological variation among early placentals, identify phylogenetically informative features, and decipher how the survival and diversification of these mammals might be related to neurosensory biology.

Here, we describe the neurosensory system of *Chriacus pelvidens* and *Chriacus baldwini*, which belong to 'Arctocyonidae', a diverse cluster of 'condylarths'. 'Arctocyonids' were among the first placental groups to diversify after the end-Cretaceous mass extinction. They have been reconstructed as small-to-medium-sized omnivores with a variety of diets, including carnivory, insectivory and frugivory (Collinson & Hooker, 1987; Archibald, 1998; Rose, 2006; Penkrot, 2010; Hooker & Collinson, 2012). Most were probably terrestrial but some may have been scansorial, cursorial or arboreal (Rose, 1996, 2006). Thus far, their fossils have been found in Europe, North America and possibly in Asia (e.g. Russell, 1964; Russell & Zhai, 1987; Williamson & Lucas, 1993). Their taxonomic history is complicated and today they are recognized as polyphyletic or as an 'ancestral stock' from which many other Paleogene mammals emerged, with some species implicated in the origins of some of the extant orders. *Chriacus* has been associated tenuously with artiodactyls (e.g. Van Valen, 1971, 1978; Rose, 1996; Ladevèze et al., 2010; De Bast & Smith, 2013),

although some studies make a link with Ferae (carnivorans and creodonts: Halliday et al., 2017). *Chriacus* was also a diverse and abundant taxon in North America during the early Paleogene, making it an important component of these early placental-dominated faunas. Thus, a description of the neurosensory anatomy of *Chriacus* has the potential to clarify aspects of the relationships, evolution and biology of the earliest placentals.

Taxonomic history

'Arctocyonidae' was once thought to belong to the carnivoran-related group Creodonta (e.g. Cope, 1875; Matthew, 1915), but the signature 'carnassials or specialized shearing teeth' (Matthew, 1937) of creodonts and carnivorans, are lacking in 'arctocyonids'. 'Arctocyonids' were then recognized as 'condylarths' and more specifically as potential stem ungulates (e.g. Patterson & Mac Grew, 1962; Van Valen, 1966 but see also Ameghino, 1901; Kretzoi, 1943; Rose, 1996; Kondrashov & Lucas, 2004a,b; De Bast & Smith, 2013). 'Arctocyonids' are divided into three subfamilies: Arctocyoninae (Matthew, 1937), Loxolophinae (Van Valen, 1978) and Oxyclaeninae (Matthew, 1937; see also Cifelli, 1983). The relationships among these subfamilies have long been under debate (see Simpson, 1945; Van Valen, 1978; Prothero et al., 1988; Archibald, 1998; Rose, 2006) and 'Arctocyonidae' is almost certainly not a monophyletic group (Archibald, 1998; Williamson & Carr, 2007; De Bast & Smith, 2013). Evolutionary relationships among 'arctocyonids' remain to be properly tested by a large-scale phylogenetic analysis including Mesozoic, Paleogene and extant mammals, which is ongoing in our research group.

The 'arctocyonid' *Lipodectes pelvidens* was first described by Cope (1881b) and two years later he referred this species to the new genus *Chriacus*. Currently, *Chriacus* is composed of nine different species (Archibald, 1998) and thus far no phylogenetic analysis has untangled the relationships among those species or even tested whether they all form a clade or even constitute a single genus. Thus, the genus *Chriacus* likely needs to be revised (Williamson & Lucas, 1993), but this is outside of the scope of our study. In general, the specimens assigned to *Chriacus* indicate a mammal similar in size to a raccoon (~ 5–10 kg; Rose, 1987), which was probably scansorial to arboreal or even cursorial, depending on the specimens being studied (Rose, 1996, 2006). Specimens of *Chriacus* are known from the early Paleocene (Pu2) to the late Eocene (Archibald, 1998) and, unusually for a Paleogene 'archaic' placental, include a large amount of associated cranial and postcranial material (Matthew, 1897, 1915; Rose, 1987, 1990, 1996; Szalay & Lucas, 1996).

A close relationship between *Chriacus* and Artiodactyla has been proposed, based on both postcranial and dental elements (Van Valen, 1971, 1978; Rose, 1996). This has been corroborated by some recent phylogenetic analyses, most notably the study of Ladevèze et al. (2010), which found *Chriacus* nested inside the sister-clade to Artiodactyla (including the oldest unequivocal extinct artiodactyl, *Diacodexis*), and the analysis of De Bast & Smith (2013), which placed it within an array of 'condylarths' closely related to *Diacodexis*. However, a *Chriacus*-artiodactyl link is by no means certain: Rose (1987) argued that postcrania from another *Chriacus* species of uncertain identification (referred to as *Chriacus* sp. in his study) bore little resemblance to *Diacodexis* and the phylogenetic analysis of Halliday et al. (2017) placed *Chriacus* far distant from artiodactyls, instead within a clade that includes Ferae (extant pangolins and carnivorans).

Institutional abbreviations

AMNH, American Museum of Natural History, New York, NY, USA; AMNH FM, American Museum of Natural History, Fossil Mammals, New York, NY, USA; AMNH VP, American Museum of Natural History, Vertebrate Paleontology, New York, NY, USA; MCZ, Museum of Comparative Zoology, Cambridge, MA, USA; MHNC, Museo de Historia Natural 'Alcide d'Orbigny', Cochabamba, Bolivia; NMMNH P, New Mexico Museum of Natural History, Paleontology, Albuquerque, NM, USA; PSS-MAE, Collections of Joint Paleontological and Stratigraphic Section of the Geological Institute, Mongolian Academy of Science, Ulaanbaatar – American Museum of Natural History, New York, NY, USA; UFRJ-DG, Universidad Federal do Estado de Rio de Janeiro, Rio de Janeiro, Departamento de Geologia, Brazil; USNM, United States National Museum, Washington, DC, USA.

Materials and methods

Chriacus specimens

The *Chriacus* specimens studied here belong to two different species: *Ch. baldwini* and *Ch. pelvidens*. A large amount of material has been attributed to *Ch. baldwini*, including postcranial material (Matthew, 1897; *Chriacus truncatus* in Rose, 1996). This species was first described by Cope (1882) and subsequently many other species of *Chriacus* have been synonymized with *Ch. baldwini* (see Williamson & Lucas, 1993). A variety of mandibular and dental elements have been described for *Ch. pelvidens* (see Matthew, 1897, 1937; Gazin, 1969; Krause & Gingerich, 1983; Kondrashov & Lucas, 2015). We analyzed two specimens: a cranium (MCZ 20676) belonging to *Ch. baldwini* and two petrosals (NMMNH P-62258) pertaining to *Ch. pelvidens*, which have been found associated with cranial and postcranial material, including teeth diagnostic for the species. We use these specimens to describe the brain and inner ear endocasts of *Chriacus*. As noted above, the genus *Chriacus* is in need of revision (Williamson & Lucas, 1993). The petrosals studied here exhibit

divergent morphologies, which might result in generic reclassification upon broader revision.

Cranium

MCZ 20676 is slightly flattened dorsoventrally but most of the cranium is preserved (Fig. 1, SI., Supporting Information Fig. S1). The specimen lacks fine details such as bone sutures on its surface. A large hole penetrates the specimen medial to the auditory region (Fig. 1). Neither zygomatic arch is preserved. The external aspect of the auditory region is better preserved on the right side of the cranium and some foramina can be identified (Fig. 1A). The molars M1 to M3 are preserved on both sides and are not very worn, but the occlusal surface of both P5s is strongly damaged (Fig. 1A). MCZ 20676 was collected by Craig Wood in 1980, but the exact locality was not recorded. Stratigraphically, the location is similar to the position of locality 9 at Escavada Wash of the Nacimiento Formation of the San Juan Basin, New Mexico, but possibly lower (early Paleocene; Torrejonian NALMA; To2, ~62.7–62.6 Ma; Leslie et al. 2018). The two species present in the Torrejonian age deposits of the Nacimiento Formation, *Ch. pelvidens* and *Ch. baldwini*, are very similar morphologically but are of different size, with *Ch. pelvidens* larger (Williamson & Lucas, 1993; Williamson, 1996). One of the most diagnostic characteristics of M1-2 in MCZ 20676, a feature that readily allows confident identification as *Chriacus*, is the hypertrophied hypocone that forms a lobe that extends distolingually. The hypocone lobe projects far lingual to the margin of the protocone. This specimen has never been described in detail; however, based on size, we assign it to *Ch. baldwini*.

Petrosals

NMMNH P-62258 includes the left and right petrosals of a single individual (Fig. 2). Some of the foramina of the ear region are visible, such as the fenestra vestibuli and external aperture of the cochlear fossula (Fig. 1B). This specimen also includes a fragmented partial cranium, mandibles and associated fragmented postcrania. The dentition is incomplete and includes three isolated incisors, a partial left dP5, a left M1, a fragmented right m1, partial right m2 and numerous fragments of other upper and lower teeth. Several fragments of the mandibles are unusually shallow and have immature bone grain, confirming that NMMNH P-62258 was a juvenile. This specimen has yet to be described in detail and was collected by U. Denetclaw and T.E.W. in 2010 from locality L-4950, which is on the East Flank of Torreon Wash in the Nacimiento Formation (early Paleocene; Torrejonian NALMA; To2, ~ 62.63 Ma; Leslie et al. 2018). Solely based on size, the teeth associated with the petrosal can be attributed to *Ch. pelvidens*.

Comparative sample

For morphological comparisons of the inner ear, we made comparisons to the Eocene artiodactyl *Diacodexis ilicis* (AMNH VP 16141; Orliac et al., 2012b), the potential Paleocene stem euungulate *Protungulatum* sp. (AMNH VP 118359; Orliac & O'Leary, 2016), two specimens of the Paleocene pantodont *Alcidedorbignya inopinata* (MHNC 8399; MHNC 8360; Muizon et al., 2015), the Paleocene periptychid 'condylarth' *Carsioptychus coarctatus* (AMNH 27601; Cameron et al., 2019), and the Eocene 'condylarth' *Hyopsodus lepidus* (AMNH FM 143783; Ravel & Orliac, 2015). For quantitative measurements, in addition to the specimens above, we made comparisons with Late Cretaceous eutherians: *Ukhaatherium gobiensis* (PSS-MAE 110; Ekdale, 2013), *Kulbeckia kulbecke* (average values), *Zalambdalestes lechei* (average values) and zhelestids (average values; Ekdale & Rowe, 2011). For agility score comparisons, we also included

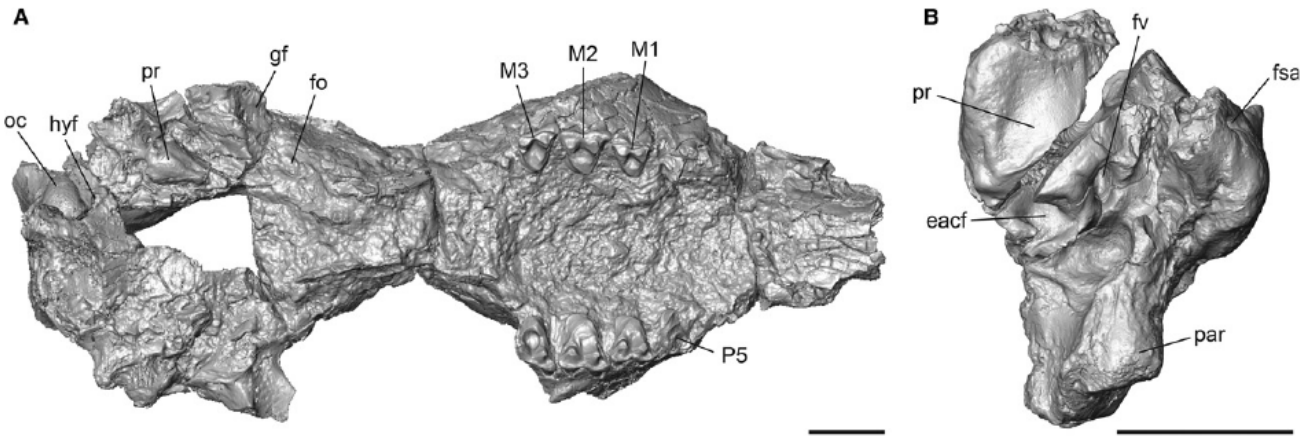

Fig. 1 The cranium of *Chriacus baldwini* (MCZ 20676) and inner ear of *Chriacus pelvidens* (NMMNH P-62258). (A) Ventral view of the cranium of MCZ 20676 (by permission of the Harvard Board of Trustees), and (B) ventral view of the left petrosal of NMMNH P-62258. All images are surface renderings from CT scan data. Scale bars: 5 mm. eacf, external aperture of cochlear fossula; fo, foramen ovale; fsa, foramen for ramus superior of stapedial artery; fv, fenestra vestibuli; gf, glenoid fossa; hyf, hypoglossal foramen; M, molar; oc, occipital condyle; P, premolar; par, paroccipital process of petrosal; pr, promontorium of petrosal.

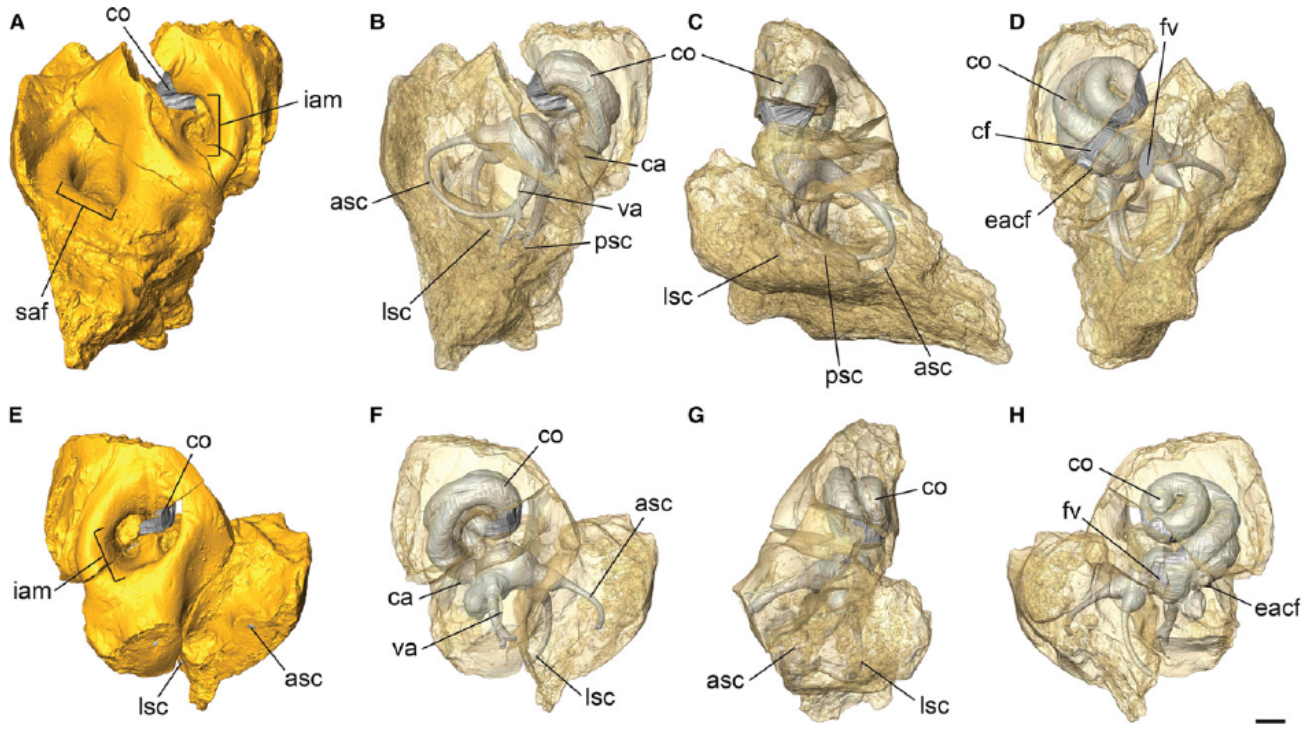

Fig. 2 Virtual endocasts of the bony labyrinth inside the petrosal bones of *Chriacus pelvidens* (NMMNH P-62258). Specimen illustrated in (A–D) is the left ear and (E–H) is the right ear. (A,B,E,F) dorsal, (C,G) anterolateral and (D,H) ventrolateral views. Scale bar: 1 mm. asc, anterior semicircular canal; ca, cochlear aqueduct; co, cochlear canal; cf, cochlear fossula; eacf, external aperture of cochlear fossula; fv, fenestra vestibuli; iam, internal acoustic meatus; lsc, lateral semicircular canal; psc, posterior semicircular canal; saf, subarcuate fossa; va, vestibular aqueduct.

Paleocene and Eocene plesiadapiforms and euprimates (Supporting Information Table S4; Silcox et al., 2009a). For hearing frequency comparisons, we also included extant taxa from Ekdale (2013; see Supporting Information Table S5). For anatomical comparisons of the cranial endocast, we compared our specimens with *Diacodexis ilicis* (AMNH VP 16141; Orliac & Gilissen, 2012), *Hyopsodus lepidus* (AMNH FM 143783; Orliac et al., 2012a), *Alcidedorbignya inopinata* (MHNC 8372; Muizon et al., 2015), *Carsioptychus coarctatus* (AMNH 27601) and the Paleocene taeniodont *Onychodectes tisonensis* (AMNH 785; Napoli et al., 2018).

Virtual endocasts acquisition

The petrosals of NMMNH P-62258 were scanned by I.B.B. with an X-ray microtomography instrument constructed in-house at the University of Edinburgh School of GeoSciences. Both petrosals were scanned with the following parameters: voltage of 120 kV, current of 23 μA and voxel size of 0.014584 mm. The cranium MCZ 20676 was scanned by Justin Gladman at the Shared Materials Instrumentation Facility (SMIF), Duke University in Durham, NC, USA. This specimen was flipped right/left during the scanning process. The inside of the cranium is not well preserved and identifying the boundary between bone and matrix was challenging (Supporting Information Fig. S2A). MCZ 20676 was scanned with the following parameters: voltage of 220 kV, current of 118 μA and voxel size of 0.0267349443551745 mm. The three specimens were segmented in Avizo® 9.7.0 software (Visualization Sciences Group, 1995–2018). New LabelField modules were created to segment the different specimens. The pen tool was used to isolate the endocranial cavity of the petrosals and cranium because the inside was not empty and the matrix had similar density to the bone. When the bone was not preserved, a straight line was used to link the two nearest pieces of bone. If the bone was detached from the matrix, the latter was used to trace the endocast on the premise that a natural endocast had formed inside the cranium and the isolated petrosal bones. Finally, the cranium and petrosal bones and their respective endocasts were opened separately in Avizo in order to obtain an image showing the bony labyrinth and cranial endocasts inside translucent petrosals and cranium (Figs 2 and 3). For nomenclature, we followed Wible et al. (2009) and Muizon et al. (2015) and references therein for cranial and petrosal anatomy, Bertrand et al. (2018b) for endocranial anatomy and Orliac & O'Leary (2016) for bony labyrinth anatomy.

The volumes of the cochlea, labyrinth and cranial virtual endocasts were obtained by generating a surface rendering of the endocasts using unconstrained smoothing for the *Chriacus* specimens. Cochlear related measurements were recorded only for the NMMNH P-62258 bony labyrinth because of the incomplete preservation of this region in

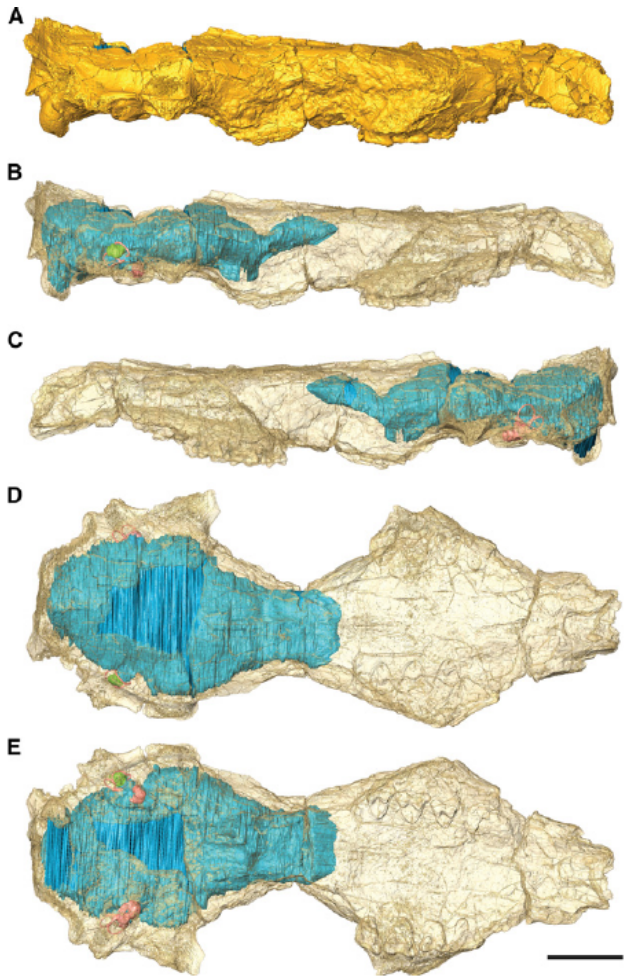

Fig. 3 Cranial and bony labyrinth virtual endocasts inside the cranium of *Chriacus baldwini* (MCZ 20676). (A,B) Lateral right, (C) lateral left, (D) dorsal and (E) ventral views. Scale bar: 10 mm (by permission of the Harvard Board of Trustees).

MCZ 20676. The volume of the cochlea was acquired by isolating this structure, using the module 'volume edit' in Avizo. The stapedial ratio is used as a proxy for the area of the footplate of the stapes and corresponds to the maximal length by the maximal width of the fenestra vestibuli (Segall, 1970; Ekdale, 2013; Orliac & O'Leary, 2016). This dimension was obtained for the NMMNH P-62258 left bony labyrinth only and measured directly on the CT data and not on the 3D model of the inner ear, as we wanted to measure the rim where the stapes sits and not the fossula rim. We also measured the cochlear ratio for both NMMNH P-62258 inner ears, which was obtained by dividing the height by the width of the cochlea (Ekdale & Rowe, 2011; Ekdale, 2013). The cochlear coil, numbers of cochlear turns, the cochlear canal length and the secondary lamina coil were measured for the NMMNH P-62258 right inner ear only because of the incomplete preservation of this region in MCZ 20676. To estimate the cochlear coil and numbers of cochlear turns, we referred to Ekdale (2009), who followed the method of Geisler & Luo (1996). At the base of the cochlea, we drew a line from the intersection between the primary and secondary bony laminae, and passing through the center of the cochlea. Half a turn was counted each time the line was crossed. An angle was then added for the remainder of the cochlear canal (see Supporting Information Table S1). The number of turns corresponds to the total angle divided by 360°. The cochlear canal length (= basilar membrane length; Ekdale & Rowe, 2011) was calculated using the function *Spline Probe* (Ekdale, 2013) in Avizo. The measurement corresponds to the distance from the region where the basilar membrane (primary and secondary laminae junction) is visible, to the apex of the cochlea. The secondary lamina coil was calculated in a similar manner to the cochlear coil (Table S1). The area including the lamina coil corresponds to the extent of the secondary bony lamina. The laminar gap corresponding to the connection between the primary and secondary laminae (= basilar membrane) on the cochlear canal (Meng & Fox, 1995; Orliac & O'Leary, 2016) was determined on the NMMNH P-62258 left inner ear only. Additional dimensions of the semicircular canals were taken on the NMMNH P-62258 and MCZ 20676 left inner ears in Avizo. Angles between each semicircular canal were measured following Ekdale (2009) and the height and width of each canal was measured using Ekdale's (2013: fig. 3e) method. The radius of curvature was calculated with the following equation: [0.5*((h + w)/2)] (Table S1; Spoor & Zonneveld, 1998), where h is the height of the canal and w is the width (see Ekdale, 2013; : fig.3d). The length of the canals was calculated in a similar manner to the cochlear length using the function *Spline Probe* (Ekdale, 2013) in Avizo.

Paleobiological calculations

Body mass estimation

Body mass is a metric integral to organismal biology and it is required to obtain agility scores, hearing frequency limits and the encephalization quotient. There are many different equations to estimate mammalian body mass based on teeth. Here, we use the Legendre (1989) and Damuth (1990) equations (Table 1) because the samples used to build these equations include mammals with a broad array of body masses and dental morphologies. As our *Chriacus* specimens preserved complete upper teeth only, we used a sample of other lower m1 specimens from the Nacimiento Formation of New Mexico belonging to *Ch. pelvidens* and *Ch. baldwini*. Length and width (mesial and distal) were taken on 38 specimens for *Ch. pelvidens* and 19 specimens for *Ch. baldwini* by T.E.W. (Supporting Information Tables S2 and S3). Two body mass estimates (minimum and maximum m1 areas) were calculated based on the Legendre (1989) equation and two (minimum and maximum m1 length) based on the Damuth (1990) equation for each species (see Tables 1 and 2). This gives a range of plausible body masses for *Chriacus*; we used the average for each species in the calculations below.

Locomotor agility scores

Agility scores were estimated using the equations from Silcox et al. (2009a) and were obtained for both *Ch. pelvidens* (NMMNH P-62258) and *Ch. baldwini* (MCZ 20676). The equations are presented in Table 1 and include two variables: body mass and the radius of the semicircular canals (anterior, posterior, lateral and average). These equations are based on the work of Spoor et al. (2007), which used data from extant mammals (from slow [1] to fast (6) moving mammals) to estimate the agility scores of fossil specimens. The theory behind those equations is related to the function of the semicircular canals, which are part of the vestibular system and play the role of maintaining balance while moving. During head movements, the endolymph fluid inside the semicircular canals stimulates the hair cells of the ampulla, which sends a signal to the brain and in turn stabilizes the head, and more specifically vision (Muller, 1994; Schwarz & Tomlinson, 1994; Spoor et al., 2007; Silcox et al., 2009a; Malinzak et al., 2012). The sensitivity of the semicircular canals will be increased with larger arc size (Oman et al., 1987; Muller, 1994). When body mass is taken into consideration, fast-moving animals such as fast arboreal species have a larger canal radius, and consequently higher agility scores compared with taxa moving more cautiously (Spoor & Zonneveld, 1998; Spoor et al., 2007). Table S4 includes calculated agility scores for extinct mammals using the four equations (each canal and average) for comparative purposes.

Hearing frequency

We calculated the low- and high-frequency range for the left ear of NMMNH P-62258, *Ch. pelvidens*. Three different equations were used to estimate hearing range. The equations are summarized in Table 1. West (1985) created equations that take into account the number of cochlear turns and basilar membrane length. Rosowski's (1992) equations are based on the footplate area (fenestra vestibuli dimensions). The third set of equations uses solely the basilar membrane length (Rosowski & Graybeal, 1991; Rosowski, 1992). When sound waves penetrate the ear and stimulate the stapes in the fenestra vestibuli, endolymphatic and perilymphatic fluids displace the basilar membrane from the base to the apex of the cochlea. This results in electrical signals transmitted through branches of cranial nerve VIII to the brain (Ekdale, 2016). The detection of low-frequencies occurs in the apex, whereas high-frequencies are detected at the base of the cochlea (Ekdale, 2016). This means that an increase in cochlear length would improve the sensitivity to low frequencies (Ekdale, 2016). The basilar membrane is a soft tissue and therefore is not preserved in fossils. Because this membrane runs throughout the entire cochlea in life, we used cochlear length as a proxy (Ekdale & Rowe, 2011). Supporting Information Table S5 includes calculated hearing frequency for extant and extinct mammals using the three equations for comparison purposes.

Agility scores and hearing frequency for *Ch. pelvidens* were based on NMMNH P-62258, which is a juvenile specimen. Mennecart & Costeur (2016) showed that the morphology of the inner ear of tragulid ruminants was similar

Table 1 Equations used to calculate the body masses, agility scores and hearing range of *Chriacus*

	Equations		References
Body mass	Grams and natural logarithm	X = EXP(1.7054 × (LN(m1 area)) + 2.247)	Legendre (1989) - All Mammal curve
	Grams and the logarithm with base 10	X = 10^(3.17 × (LOG10(m1 length)) + 1.04)	Damuth (1990)
Agility scores	Anterior semicircular canal	X = 10^(0.85 − 0.153 × (LOG10(BM)) + (0.706 × (LOG10(ASCR)))	Silcox et al. (2009a)
	Posterior semicircular canal	X = 10^(0.881 − 0.151 × (LOG10(BM)) + (0.677 × (LOG10(PSCR)))	
	Lateral semicircular canal	X = 10^(0.959 − 0.167 × (LOG10(BM)) + (0.854 × (LOG10(LSCR)))	
	Average semicircular canal	X = 10^(0.948 − 0.188 × (LOG10(BM)) + (0.962 × (LOG10(SCR)))	
Hearing capacity	Low-frequency limit (kHz)	X = 13 × (BML)^(−1.2)	Rosowski & Graybeal (1991) and Rosowski (1992)
	High-frequency limit (kHz)	X = 391 × (BML)^(−0.85)	
	Low-frequency limit (kHz)	X = 0.4 × (FP)^ −1.1	Rosowski (1992)
	High-frequency limit (kHz)	X = 34 × (FP)^ −0.4	
	Low-frequency limit (kHz)	X = 10^(1.76 − 1.66 × LOG10(CT × BML))	West (1985)
	High-frequency limit (kHz)	X = 10^(2.42 − 0.994 × LOG10(CT / BML))	

ASCR, anterior semicircular canal radius (mm); BM, body mass; BML, basilar membrane length; CT, number of cochlear turns; EXP, exponential; FP, footplate area based on the fenestra vestibuli dimensions; LN, natural logarithm; LOG10, logarithm with base 10; LSCR, lateral semicircular canal radius (mm); PSCR, posterior semicircular canal radius (mm); SCR, average semicircular canal radius (mm).

Table 2 Estimated body masses for *Chriacus pelvidens* (NMMNH P-62258) and *Chriacus baldwini* (MCZ 20676) based on the equations from Table 1

Equation	BM (area) min	BM (area) max	BM (L) min	BM (L) max
Legendre (1989)	**1827.48**	5368.04	–	–
Damuth (1990)	–	–	3211.73	**7082.32**
Average BM *Ch. pelvidens* = 4372.39 g				

Equation	BM (area) min	BM (area) max	BM (L) min	BM (L) max
Legendre (1989)	**643.95**	2274.77	–	–
Damuth (1990)	–	–	1201.56	**3211.73**
Average BM *Ch. baldwini* = 1833.00 g				

BM, body mass; L, length.
Dental measurements are available in Tables S2 and S3. Values in bold are upper and lower estimates. Average body mass was calculated based on the four estimated body masses for each species.

between adult and juvenile specimens. Therefore, we expect that the morphological and quantitative conclusions obtained here for the juvenile NMMNH P-62258 should be similar to the results obtained for an adult.

Encephalization quotient

The encephalization quotient is used to compare brain size among specimens exhibiting different body masses. This encephalization quotient ($EQ = E_i/E_c$) was first proposed by Jerison (1973) and corresponds to the ratio between the actual brain size (E_i) of a given species (i) and the brain size expected for a hypothetical 'typical' mammal of the same body mass (E_c; Martin, 1990). To obtain the EQ of MCZ 20676, we used Jerison's (1973) equation: $E_i/(0.12 \times (E_c)^{0.67})$ and Eisenberg's (1981) equation: $E_i/(0.0553 \times (E_c)^{0.74})$ for the calculation of E_c, which are derived from broad taxonomic samples. We provided an EQ range for MCZ 20676 to reflect the uncertainty of the body mass (Table 3, Supporting Information Table S6). We used the EQs based on Jerison's (1973) equation for comparison purposes in Table S6 only.

Neurobiology

Volumes were calculated for two different portions of the cranial endocast of MCZ 20676, *Ch. baldwini*. The volume of the olfactory bulbs was obtained in a similar manner to the cochlear volume, and the petrosal lobules (= paraflocculi) were re-segmented to obtain volumetric measurements. The term petrosal lobule is used over paraflocculus because it defines more accurately the functional portion of the cerebellum that is located in the subarcuate fossa. For example, in primates, only a portion of the paraflocculus is housed in the subarcuate fossa (Gannon et al., 1988; Hiramatsu et al., 2008), whereas in rodents, the entire paraflocculus fills the fossa (McClure & Daron, 1971; Sakamoto et al., 2017).

For MCZ 20676, the XY dimension was used to isolate the right petrosal lobule. The left auditory region was too damaged to isolate the petrosal lobule on this side. For the left ear of NMMNH P-62258, the YZ dimension was used to isolate the petrosal lobule. Because the neocortex was incomplete, we used neocortical height ratio as a proxy for neocortical surface area ratio. This method was used by Bertrand et al. (2018a,b) because, in their study, some specimens lacked a completely preserved neocortex; importantly, they found that neocortical height was strongly correlated with neocortical surface area ratio in rodents (Table 3).

Analysis for potential phylogenetically informative characters

Many features of the bony labyrinth likely have phylogenetic significance. In the future, we will incorporate a suite of neurosensory characters (mainly related to the bony labyrinth) into the large-scale phylogenetic analysis of mammals that our group is working on, but this is outside the scope of this paper. Here, to investigate the distribution of major bony labyrinth features among early placental mammals and to assess potential synapomorphies, we use a modified version of the character dataset of Macrini et al. (2013). Like those authors, we do not use this limited dataset to perform a phylogenetic analysis here, as the results of an inner ear-only character analysis likely would not provide an accurate phylogeny.

Our modifications make the dataset more inclusive for understanding the distribution of inner ear features in early placentals and close relatives. We scored *Ch. pelvidens* and *Ch. baldwini* for the dataset, and also added other taxa: *D. ilicis* (AMNH VP 16141; Orliac et al., 2012b), *Protungulatum* sp. (AMNH VP 118359; Orliac & O'Leary, 2016), *A. inopinata* (MHNC 8372; Muizon et al., 2015), *Ca. coarctatus* (AMNH 27601) and the litoptern indet. UFRJ-DG 1035-M (Billet et al., 2015; Table 4). We also added several new states for characters to better encapsulate variation present in early placental mammals, which was not parsed out in the Macrini et al. (2013) dataset, as it was designed to understand character distribution in Notoungulata. Based on our observations, we added one new state to each of the following characters: anterior and lateral ampullae position (#9), utricle and saccule housing (#15), position of chamber for utricle (in bony labyrinth) when viewed dorsally (#16), and two new states to one character: diameter of fenestra cochleae relative to that of fenestra vestibuli (#25; Table 5). Additionally, we modified the coding of some characters for certain taxa, including: *Hyopsodus* using *H. lepidus* (AMNH FM 143783; Ravel & Orliac, 2015); a notoungulate indet. (MNHN-F-BRD 23 of Billet & Muizon, 2013); the notoungulate *Notostylops*

Table 3 Inner ear and brain quantification summary for *Chriacus pelvidens* (NMMNH P-62258) and *Chriacus baldwini* (MCZ 20676) compared with Paleocene and Eocene placental mammals

	Ch. baldwini (MCZ 20676)	*Ch. pelvidens* (NMMNH P-62258; Left ear)	*Diacodexis ilicis* (AMNH VP 16141)	*Hyopsodus lepidus* (AMNH FM 143783)	*Alcidedorbignya inopinata* (MHNC 8399, 8360, 8372)	*Carsioptychus coarctatus* (AMNH 27601)	*Protungulatum* sp. (AMNH VP 118359)
Endocranial volume (mm^3)	2699.42	–	4700	2790	2203.22	–	–
Olfactory bulb volume (mm^3)	187.0	–	320	240	187.1	–	–
Petrosal lobule volume (mm^3)	6.88	–	36.61	6.60	–	–	–
Neocortical height (mm)	2.04	–	22.50	20.38	13.62	–	–
Endocranial height (mm)	8.21	–	71.84	61.04	66.32	–	–
Olfactory bulb percentage ratio (%)	6.93	–	6.81	8.60	8.49	–	–
Petrosal lobule percentage ratio (%)	0.25	–	0.78	0.24	–	–	–
Neocortical percentage ratio (%)	24.85	–	31.32	33.39	20.54	–	–
Encephalization quotient	0.12–0.41	–	0.54–0.79	0.34–0.70	0.36–0.49	–	–
Agility score	2.09–2.86	2.62–3.46	3.48–3.84	3.12–3. 74	2.83–3.06	2.39–2.74	3.35–3.62
Low- and high-frequency limits of hearing	–	0.32–40.29	0.64–73.73	0.33–57.82	(0.56–0.84) to (36.76–47.01)	0.61–47.78	1.09–57.43

Data for comparative sample are from Cameron et al. (2019), Orliac & O'Leary (2016), Ravel & Orliac (2015), Muizon et al. (2015), Orliac & Gilissen (2012) and Orliac et al. (2012a). Neocortical and endocranial heights, petrosal lobule and endocranial volumes were measured directly on the cranial endocasts published by Orliac & Gilissen (2012) and Orliac et al. (2012a). For Muizon et al. (2015), neocortical and endocranial heights were measured on published figures. The petrosal lobule volume percentage ratio is for two petrosal lobules. Low- and high-frequency limits of hearing at 60 dB in kHz are based on the equation from West (1985). Agility scores are based on the average semicircular canal. Body masses used for the encephalization quotients and agility scores are available in Tables S4 and S6.

(Macrini et al., 2010); and *Ca. coarctatus* (AMNH 27601; see Table 4).

Our modified dataset now includes 25 characters scored for 18 taxa. We elected not to map the characters onto a preexisting tree topology because, currently, there is no consensus for the phylogenetic position of many of our taxa. Instead, we comment here on similarities between taxa that could potentially be informative when integrated later into a phylogenetic analysis.

Descriptions and comparisons

Cranial endocast

The anterior aspect of the cranial endocast of *Ch. baldwini* (MCZ 20676), including the forebrain (cerebrum and olfactory bulbs), is slightly crushed dorsoventrally (Figs 3 and 4).

Olfactory bulbs

In dorsal view, the olfactory bulbs of *Ch. baldwini* (MCZ 20676; Fig. 4A) have an elliptical shape similar to those of *H. lepidus* (AMNH FM 143783; Fig. 5C) and *A. inopinata* (MHNC 8372; Fig. 5D). This contrasts with *D. ilicis* (AMNH VP 16141), in which the olfactory bulbs have a more triangular shape (Fig. 5B). The olfactory bulbs are conjoined in *Ch. baldwini* (MCZ 20676; Figs 4A and 5A) and all other compared specimens (Fig. 5). *Chriacus baldwini* (MCZ 20676) has olfactory bulbs representing about 6.9% of the total endocranial volume (Table 3). The volume percentage for the olfactory bulbs of *Ch. baldwini* (MCZ 20676) is similar to those of *D. ilicis* (6.8%; AMNH VP 16141; Orliac & Gilissen, 2012) but lower than those of *H. lepidus* (8.6%; Orliac et al., 2012a) and *A. inopinata* (8.5%; MHNC 8372; Muizon et al., 2015). The volume of the olfactory bulbs was not recorded for the other specimens. For other

Table 4 Taxon-inner ear character matrix (modified from Macrini et al., 2013)

	1	2	3	4	5	6	7	8	9	10	11	12	13	14	15	16	17	18	19	20	21	22	23	24	25
Caluromys	0	0	0	0	0	0	0	0	0	1	1	0	0	0	0	0	?	0	0	0	0	0	0	0	0
Ukhaatherium	0	0	0	0	1	0	0	0	1	?	?	?	0	0	?	?	?	?	?	1	0	0	1	?	?
Kulbeckia	0	0	0	0	1	0	1&2	0	0	1	1	0	1	0	?	?	?	?	?	0&1	0	0	1	?	?
Zalambdalestes	0	0	0	0	1	0	1	0	0	1	1	1	1	0	?	?	?	?	?	1	0	0	1	0	?
Chilecebus	0	0	1	0	0	0	0	0	0	?	?	?	1	0	1	1	?	0	1	?	0	1	?	?	?
UFRJ-DG 1035-M*	0	0	0	0	0	0	2	0	1	1	1	0	0	1	?	?	1	0	0	0	0	0	0	?	2
MNHN-F-BRD 23	0	0	0	0	0	0	0	0	0	1	1	1	1	1	?	?	1	0	1	0	0	0	0	0	**2***
Altitypotherium	0	0	1	0	1	1	2	0	0	1	1	1	0	2	1	0	0	?	?	1	0	1	0	0	?
Pachyrukhos	0	0	1	1	1	0	0	0	0	1	1	1	1	0	1	0	1	1	1	?	1	1	0	0	1
Cochilius	1	1	0	0	0	1	0	1	1	?	?	?	1	0	1	1	?	?	?	?	0	1	?	?	?
Notostylops	0	0	0	0	0	0	1	1	0	1	1	1	1	1	1	1	0	0	1	0	1	1	0	0	**3***
Alcidedorbignya inopinata*	0	0	0	0	0	0	0	0	2	1	1	?	0	1	0	NA	1	0	0	0&1	0	0	0	0	0
Carsioptychus coarctatus	**0***	0	0	0	0	0	2	0	**2***	1	1	1	1	**2***	**0***	**NA***	?	?	?	?	0	0	?	?	?
Hyopsodus lepidus	0	1	**1***	0	0	0	**1***	0	**2***	**1***	1	?	1	0	0	**NA***	**1***	**0***	0	**0***	0	0	?	1	**3***
Diacodexis ilicis*	0	0	0	0	1	0	2	0	2	1	1	?	0	0	2	2	1	0	1	0	0	0	0	?	3
Protungulatum* sp.	0	0	0	0	1	0	0	0	2	1	1	0	1	2	2	2	1	0	0	1	0	0	0	?	2
Chriacus pelvidens*	0	0	0	0	0	0	1	0	2	1	1	0	1	0	2	2	1	0	1	1	0	0	0	?	2
Chriacus baldwini*	0	0	0	0	0	0	0	0	2	1	1	0	1	0	2	2	0	?	?	?	0	0	?	0	?
Reconstructed Placental Ancestor	0	0	0	0	0	0	0	0	0	1	1	0&1	1	0	0&1	1	0&1	0	0&1	0&1	0	0&1	0&1	0	0

NA, non-applicable.

States in bold and accompanied by an asterisk have been modified from original matrix; taxa in bold and accompanied by an asterisk are newly coded specimens. All the specimens are fossils except the opossum *Caluromys*. MNHN-F-BRD 23 is a notoungulate indet. from Billet & Muizon (2013) and UFRJ-DG 1035-M is a litoptern indet. from Billet et al. (2015). The 'Reconstructed Placental Ancestor' coding corresponds to the ancestral condition reconstructions from Macrini et al. (2013) but the character optimization might change with the addition of these new taxa.

Table 5 Character list used to build the matrix (see Table 5)

1	Lateral reach of LSC and PSC: (0) equivalent; (1) LSC terminates more medially than PSC (modified from Schmelzle et al. 2007, character #4).
2	Form of LSC in its transition to the lateral ampulla: (0) straight; (1) undulating (Schmelzle et al. 2007, character #6).
3	Form of LSC at its transition to vestibule: (0) straight; (1) undulating (Schmelzle et al. 2007, character #7).
4	Posterior arm of the LSC in relation to the level of the PSC: (0) anterior or even with the level of the PSC; (1) extends posterior to the level of the PSC (modified from Schmelzle et al. 2007, character #8).
5	Shape of the PSC when viewed in the plane of the canal: (0) mostly in the same plane; (1) extends posterior to the level of the PSC (modified from Schmelzle et al. 2007, character #8).
6	Semicircular canal with largest overall radius of curvature: (0) ASC; (1) PSC (Macrini et al., 2013).
7	Roundest semicircular canal: (0) LSC; (1) PSC; (2) ASC. This is determined by comparison of length vs. width measurements of each SSC (Macrini et al., 2013). In the present study, the term 'height' is used instead of 'length'.
8	Anterior and posterior ampullae dorsoventral girth relative to semicircular canal cross-sectional diameter: (0) ampullae girth in the dorsoventral direction extend well beyond the SSC boundaries; (1) ampullae are not noticeably expanded anterodorsally beyond the plane of the SSC (Macrini et al., 2013).
9	Anterior and lateral ampullae position: (0) lie in the same or nearly the same horizonal plane as the LSC; (1) anterior ampulla is significantly dorsal to the lateral ampulla; **(2) anterior ampulla is just dorsal to the lateral ampulla*** (modified from Macrini et al., 2013).
10	Primary osseous spiral lamina: (0) absent; (1) present (Meng & Fox, 1995).
11	Secondary osseous spiral lamina: (0) absent; (1) present (Meng & Fox, 1995).
12	Length of secondary osseous lamina: (0) extends well past the basal turn; (1) extends from the fenestra cochleae only through the first half of the basal turn (Luo & Eastman, 1995; Geisler & Luo, 1996; Luo & Marsh, 1996).
13	Crus commune lumen diameter thickness relative to semicircular canals: (0) crus diameter is significantly thicker than canals; (1) crus has a diameter similar to that of the canals (Macrini et al., 2013).
14	Dorsal extent of ASC and PSC above the crus commune: (0) only ASC extends well dorsal to the crus; (1) ASC and PSC both extend well dorsal to the crus commune; (2) neither canal extends well dorsal to the crus (Macrini et al., 2013).
15	Utricle and saccule housing: (0) in a common chamber; (1) within distinct, separated chambers in bony labyrinth; **(2) within distinct, but not separated chambers in bony labyrinth*** (modified from Macrini et al., 2013).
16	Position of chamber for utricle (in bony labyrinth) when viewed dorsally: (0) bulge for the utricle positioned closer to the posterior end of the LSC than the anterior end; (1) centrally located between ends of the LSC; **(2) closer to the anterior end of the LSC*** (modified from Macrini et al., 2013).
17	Thickness of canal connecting the posterior ampulla and foramen singulare (transmits nervus ampullaris posterior): (0) less than that of semicircular canals; (1) equal to or exceeds that of semicircular canals (Macrini et al., 2013).
18	Posterior end of the canal for the aqueductus cochleae: (0) extends posterior to the PSC; (1) does not extend posterior to the PSC (Macrini et al., 2013).
19	Thickness of aqueductus cochleae relative to that of the semicircular canals: (0) similar; (1) aqueductus cochleae diameter less than that of semicircular canals (Macrini et al., 2013).
20	Stapedial ratio: (0) rounded, <1.8; (1) elliptical, 1.8 or greater (Rougier et al., 1998; character #127).
21	Confluence between the inferior arm of the PSC and the posterior arm of the LSC near the mid-length of these semicircular canals: (0) absent; (1) present (Macrini et al., 2013).
22	Secondary crus commune: (0) present; (1) absent (Macrini et al., 2013).
23	Fenestra cochleae position relative to fenestra vestibuli (in lateral view of the inner ear endocast): (0) fenestra cochleae posterior to fenestra vestibuli; (1) fenestra cochleae posteromedial to fenestra vestibuli (Wible et al., 2007, character #303).
24	Fenestra cochleae orientation: (0) fenestra opens posterolaterally; (1) fenestra faces posteriorly (Bloch et al. 2007, character #106).
25	Diameter of fenestra cochleae relative to that of fenestra vestibuli: (0) fenestra cochleae is larger; (1) fenestra vestibuli is larger; **(2) equivalent*; (3) fenestra cochleae is twice as large*** (modified from Macrini et al., 2013).

ASC, anterior semicircular canal; LSC, lateral semicircular canal; PSC, posterior semicircular canal; SSC, semicircular canal (collectively). The list is modified from Macrini et al. (2013). New states are in bold and accompanied by an asterisk.

comparisons, the early Eocene ischyromyid rodent *Paramys copei* (AMNH 4756) has olfactory bulbs that represent 6.1% (Bertrand et al., 2016) and the early Eocene plesiadapiform *Ignacius graybullianus* (USNM 421608) has olfactory bulbs of 5.5% (Silcox et al., 2009b). Overall, *Ch. baldwini* (MCZ 20676) and other early placental mammals have, on average, smaller olfactory bulbs compared with Cretaceous eutherians (8.4–10%; Kielan-Jaworowska, 1984).

The olfactory bulbs are located posterior to the molars and not above them in *Ch. baldwini* (MCZ 20676; Fig. 3), *Ca. coarctatus* (AMNH 27601; Cameron et al., 2019: fig. 2d) and *Onychodectes tisonensis* (AMNH 785; Napoli et al., 2018: fig.1a). This contrasts with the condition of *D. ilicis* (AMNH VP 16141; Bertrand et al., 2016) and *H. lepidus* (AMNH FM 143783), in which the olfactory bulbs are located above the M3 (See Orliac & Gilissen, 2012: fig. 1c;

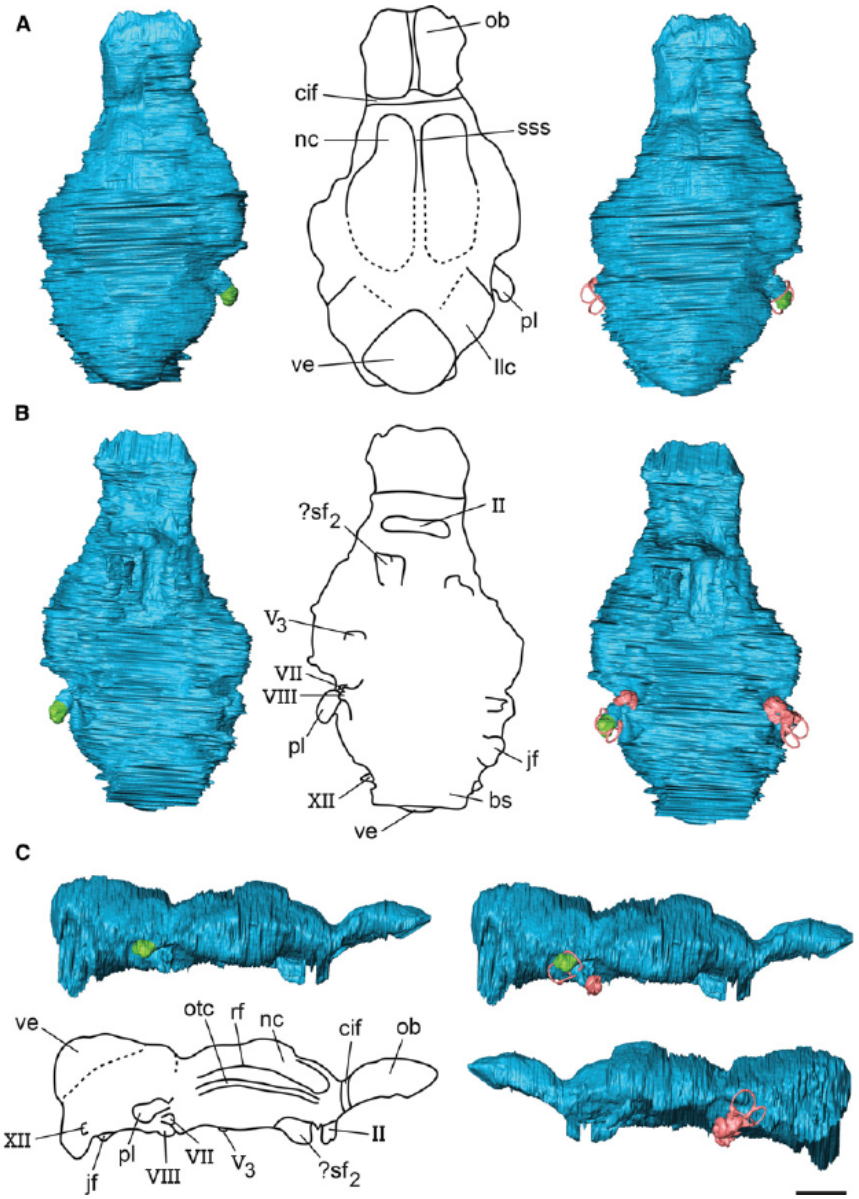

Fig. 4 Virtual reconstruction of the cranial and bony labyrinth endocasts as well as outlined drawing of the cranial endocast of *Chriacus baldwini* (MCZ 20676). (A) Dorsal, (B) ventral and (C) lateral right and left views. Scale bar: 5 mm. The petrosal lobule is in green, the rest of the endocast in blue and the bony labyrinth in pink. bs, brainstem; cif, circular fissure; jf, internal jugular vein and cranial nerves IX, X, XI; II, optic nerve; llc, lateral lobe of cerebellum; nc, neocortex; ob, olfactory bulb; otc, orbitotemporal canal; pl, petrosal lobule; rf, rhinal fissure; sf_2, ophthalmic veins and cranial nerves III, IV, V_1, V_2 and VI; sss, superior sagittal sulcus; ve, vermis; V_2, maxillary nerve; V_3, mandibular nerve; VII, facial nerve; VIII, vestibulocochlear nerve; XII, hypoglossal nerve.

Orliac et al., 2012a: fig. 2a). In *Paramys copei* (AMNH 4756), the olfactory bulbs are located above the M2, and in *I. graybullianus* above the M1 (USNM 421608; Silcox et al., 2009b: fig. 1a). This difference might be due to changes in the proportions of the skull between early placental mammals and more derived groups such as early artiodactyls, rodents and primates. This could be related to an increase in the size of the braincase compared with the anterior part of the cranium, or vice versa. *Chriacus baldwini* (MCZ 20676; Fig. 5I), *O. tisonensis* (AMNH 785; Napoli et al., 2018: fig. 2b), *A. inopinata* (MHNC 8372; Fig. 5L) and *H. lepidus* (AMNH FM 143783; Fig. 5K) have longer circular fissures compared with *D. ilicis* (AMNH VP 16141; Fig. 5J). This could reflect less anterior expansion of the frontal lobes in these specimens compared with those of *D. ilicis*.

Cerebrum and midbrain

The maximum mediolateral width of the cerebrum is greater in *Ch. baldwini* (MCZ 20676; Fig. 5A) and *H. lepidus* (AMNH FM 143783; Fig. 5C) compared with *Ca. coarctatus* (AMNH 27601; Cameron et al., 2019: fig. 3c), *A. inopinata* (MHNC 8372; Fig. 5D) and *O. tisonensis* (AMNH 785; Napoli et al., 2018: fig. 2c), but lower than in *D. ilicis* (AMNH VP 16141; Fig. 5B). On the dorsal surface of the endocast, the area where the midbrain should be located is not visible because of the poor preservation of this region and the posterior limit of the cerebrum is not clearly visible in *Ch. baldwini* (MCZ 20676; see Figs 4 and 5). In *A. inopinata* (MHNC 8372), *H. lepidus* (AMNH FM 143783) and *D. ilicis* (AMNH VP 16141), the midbrain is exposed and not covered by the cerebrum (Fig. 5).

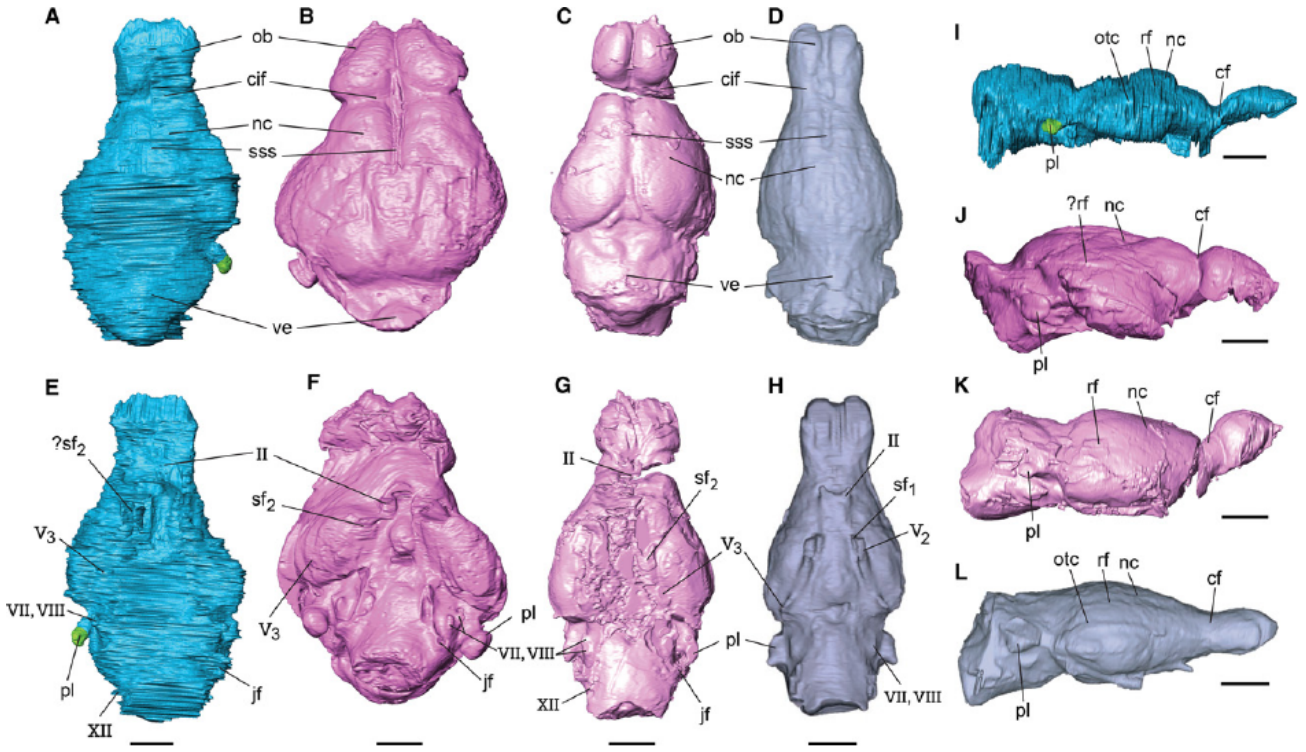

Fig. 5 Comparison of the cranial endocast morphology of *Chriacus baldwini* (MCZ 20676) to that of other early placental mammals. Taxa illustrated are (A,E,I) *Ch. baldwini* (MCZ 20676); (B,F,J) *Diacodexis ilicis* (AMNHVP 16141; Orliac & Gilissen, 2012); (C,G,K) *Hyopsodus lepidus* (AMNHFM 143783; Orliac et al., 2012a); (D,H,L) *Alcidedorbignya inopinata* (MHNC 8372; Muizon et al., 2015). Scale bars: 5 mm. (A–D) Dorsal, (E–H) ventral, (I,K,L) lateral right and (J) lateral left mirrored views. cif, circular fissure; jf, internal jugular vein and cranial nerves IX, X, XI; II, optic nerve; nc, neocortex; ob, olfactory bulb; otc, orbitotemporal canal; pl, petrosal lobule; rf, rhinal fissure; sf_1, ophthalmic veins and cranial nerves III, IV, V_1, and VI; sf_2, ophthalmic veins and cranial nerves III, IV, V_1, V_2 and VI; sss, superior sagittal sulcus; ve, vermis; V_2, maxillary nerve; V_3, mandibular nerve; VII, facial nerve; VIII, vestibulocochlear nerve; XII, hypoglossal nerve.

The rhinal fissure represents the separation between the paleo- and the neocortex on the cerebrum (Martin, 1990). This is a key landmark because it provides information on the degree of expansion of the neocortex (Jerison, 2012; Long et al., 2015). There is a relationship between the rhinal fissure and the orbitotemporal canal (sulcus) in rodents, primates and other taxa (e.g. Novacek, 1986; Martin, 1990; Silcox et al., 2010; Bertrand et al., 2018a,b). However, this relationship is not consistent across Mammalia and in some cases the rhinal fissure may occupy a more dorsal position compared with the orbitotemporal canal. In *A. inopinata* (MHNC 8372), there is a groove for the orbitotemporal canal (not annotated by Muizon et al., 2015) and dorsal to it, a ridge presumably marking the rhinal fissure (Muizon et al., 2015: fig. 55). The imprints of these cranial features are visible on the virtual cranial endocast of *A. inopinata* (MHNC 8372; Muizon et al., 2015: fig. 54 d, f). We were able to identify both of these structures in *Ch. baldwini* (MCZ 20676; see Figs 4C and 5I). As the neocortical area boundaries were not preserved well enough to calculate accurately the surface area of the neocortex, we measured the neocortical height ratio instead. *Chriacus baldwini* (MCZ 20676) has a neocortical height ratio of 24.9%, which is similar to that of *A. inopinata* (20.6%; MHNC 8372). In contrast, *H. lepidus* (33.4%; AMNH FM 143783) and *D. ilicis* (31.3%; AMNH VP 16141) show higher values (Table 3).

Cerebellum

The cerebellum of *Ch. baldwini* (MCZ 20676; Fig. 5A) is slightly narrower than the width of the cerebrum, which is similar to the condition of *A. inopinata* (MHNC 8372; Fig. 5D), *H. lepidus* (AMNH FM 143783; Fig. 5C), *D. ilicis* (AMNH FM 143933; Orliac & Gilissen, 2012: fig. S1) and *Ca. coarctatus* (AMNH 27601; Cameron et al., 2019: fig. 3c). The anterior boundary of the cerebellum cannot be distinguished in *Ch. baldwini* (MCZ 20676; Fig. 5A). The vermis and the right petrosal lobule are the only identifiable structures of the cerebellum in *Ch. baldwini* (MCZ 20676; Fig. 4). The left petrosal lobule of *Ch. pelvidens* (NMMNH P-62258) is well preserved and undeformed (Fig. 6). Both petrosal lobules have an elongated shape, which is different from that of early rodents, which have more bulbous petrosal lobules (paraflocculi in Bertrand et al., 2018a). The petrosal lobule volumes of MCZ 20676 and NMMNH P-62258 are 3.4 and 3.9 mm^3, respectively. The petrosal lobule percentage was calculated for MCZ 20676 and corresponds to ~ 0.13% of the total endocranial volume (Table 3). Two petrosal lobules would potentially represent 0.25% of the

total endocranial volume, which is similar to the 'condylarth' *H. lepidus* (AMNH FM 143783; 0.24%), the cladothere *Vincelestes neuquenianus* (0.23%; Macrini, 2006) and the mammaliform *Hadrocodium wui* (0.28%; Macrini, 2006), but below the range of early ischyromyid rodents (0.4–1.3%; Bertrand et al., 2018a), the artiodactyl *D. ilicis* (AMNH VP 16141; 0.78%) and the multituberculate *Kryptobaatar dashzevegi* (4.04%; Macrini, 2006). The petrosal lobule percentage was not calculated for *A. inopinata* (MHNC 8372; Muizon et al., 2015).

Cranial nerves and blood vessels

The preservation of fine features is limited on the ventral region of the endocast; however, several cranial nerve and blood vessel casts can be identified. The casts of the foramina for the optic nerves are visible in *Ch. baldwini* (MCZ 20676; Figs 4B and 5E) and have a similar position to those of *A. inopinata* (MHNC 8372; Fig. 5H). The primitive condition for placentals is a fusion between the foramen rotundum and the sphenorbital fissure, that is, there is no separate opening for cranial nerve V_2 (maxillary nerve) (O'Leary et al., 2013). Based on the preservation of MCZ 20676, it is impossible to determine whether the foramen rotundum (cranial nerve V_2, maxillary nerve) is confluent with the sphenorbital fissure [ophthalmic veins and cranial nerves III (oculomotor), IV (trochlear), V_1 (ophthalmic) and VI (abducens)] in *Ch. baldwini* (Figs 4B and 5E). *Alcidedorbignya inopinata* (MHNC 8372; Fig. 5H) and *Ca. coarctatus* (AMNH 27601; Cameron et al., 2019: fig. 3e) exhibit two separate foramina that appear to join anteriorly in a common fossa. This seems to contrast with the condition of *D. ilicis* (AMNH VP 16141; Fig. 5F) and *H. lepidus* (AMNH FM 143783; Fig. 5G), which have a single opening and thus a confluent foramen rotundum and sphenorbital fissure.

The mandibular nerve (V_3) would have passed through the foramen ovale in life and is visible in *Ch. baldwini* (MCZ 20676; Figs 4B and 5E), *A. inopinata* (MHNC 8372; Fig. 5H), *Ca. coarctatus* (AMNH 27601; Cameron et al., 2019: fig. 3e), *H. lepidus* (AMNH FM 143783; Fig. 5G) and *D. ilicis* (AMNH VP 16141; Fig. 5F). Casts of the internal auditory meatus, with passageways for cranial nerves VII (facial) and VIII (vestibulocochlear), are visible but not well preserved in *Ch. baldwini* (MCZ 20676; Figs 4B and 5E); however, the casts for these nerves are undeformed in the *Ch. pelvidens* left petrosal (NMMNH P-62258; Fig. 6E). The cochlear branch of cranial nerve VIII is relayed through the modiolus of the cochlea (Gray, 1907; Ekdale, 2016). The position of these casts is similar to the ones of *Ca. coarctatus* (AMNH 27601; Cameron et al., 2019: fig. 3e), *H. lepidus* (AMNH FM 143783; Fig. 5G), *D. ilicis* (AMNH VP 16141; Fig. 5F) and *O. tisonensis* (AMNH 785; Napoli et al., 2018: fig. 2b). The casts for nerves VII and VIII were not traced in *A. inopinata* (MHNC 8372; Muizon et al., 2015). The cast of the jugular foramen, which corresponds to the passageway

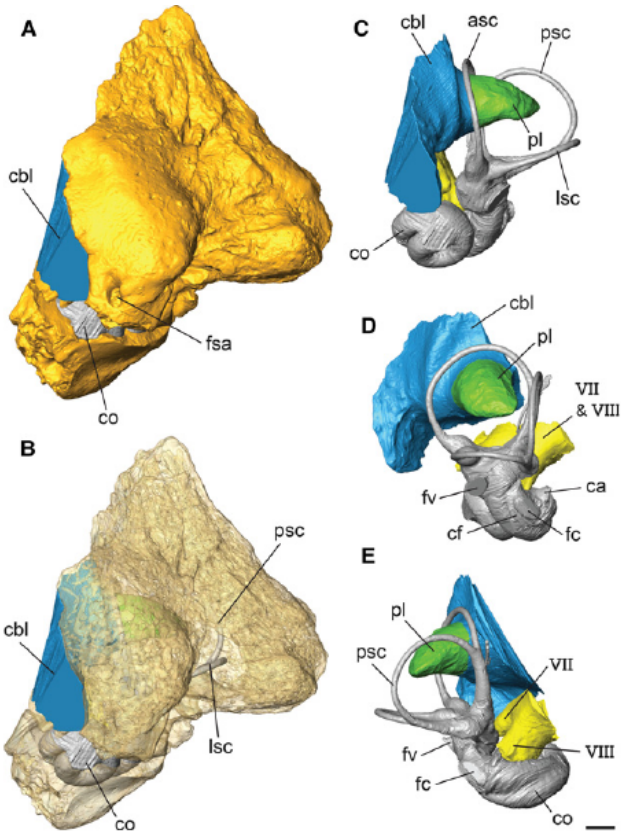

Fig. 6 Virtual endocast of the left bony labyrinth, petrosal lobule and cranial nerves VII and VIII of *Chriacus pelvidens* (NMMNH P-62258). (A, B, C, D, E) Bony labyrinth, petrosal lobule and cranial nerves VII and VIII inside the petrosal bone. (A–C) Anterolateral, (D) posterolateral and (E) oblique posterior views. Scale bar: 1 mm. asc, anterior semicircular canal; ca, cochlear aqueduct; cbl, cerebellum; cf, cochlear fossula; co, cochlear canal; fc, fenestra cochleae; fsa, foramen for ramus superior of stapedial artery; fv, fenestra vestibuli; lsc, lateral semicircular canal; pl, petrosal lobule; psc, posterior semicircular canal; VII, facial nerve; VIII, vestibulocochlear nerve. [Colour figure can be viewed at wileyonlinelibrary.com]

of the internal jugular vein and cranial nerves IX (glossopharyngeal), X (vagus) and XI (accessory), is positioned ventral to the posterior end of the petrosal lobule in *Ch. baldwini* (MCZ 20676; Figs 4B and 5E) and in the other compared specimens (Fig. 5). A single hypoglossal foramen for cranial nerve XII (hypoglossal) is preserved on each side of the endocast of *Ch. baldwini* (MCZ 20676; Figs 4B and 5E). This foramen is visible and has a similar position in *H. lepidus* (AMNH FM 143783; Fig. 5G).

Casts for vessels (arteries and veins) are not preserved in *Ch. baldwini* (MCZ 20676), except for part of the superior sagittal sinus, which is not clearly defined because of poor preservation (Fig. 4A). The superior sagittal sinus is clearly visible in better preserved specimens such as those of *D. ilicis* (AMNH VP 16141; Fig. 5B), *H. lepidus* (AMNH FM 143783; Fig. 5C) and *A. inopinata* (MHNC 8372; Fig. 5D).

Bony labyrinth endocast

Both bony labyrinths of NMMNH P-62258, as well as those of the MCZ 20676 cranium, were segmented because certain areas were better preserved on one side than on the other. The right bony labyrinth of NMMNH P-62258 is more complete in terms of the semicircular canals, whereas the cochlea is better preserved in the left bony labyrinth of the same specimen (Fig. 7). The cochlea is not well preserved in MCZ 20676, but the semicircular canals are complete on the left side (Fig. 8).

Cochlear canal

The membranous cochlea is housed in a bony structure called the cochlear canal. The length of the spiral cochlear canal is 12.3 mm for the right bony labyrinth of *Ch. pelvidens* (NMMNH P-62258), which is the longest among early placental mammals sampled (Table 6). This value is high but close to the canal length of *A. inopinata* (MHNC 8399) and *H. lepidus* (AMNH FM 143783), which measure 10.9 and 10.1 mm, respectively. The right bony labyrinth of *Ch. pelvidens* (NMMNH P-62258) exhibits 1.87 cochlear turns with a rotation of 672°, which is higher than in other sampled early placental mammals, except the Eocene *D. ilicis* (AMNH VP 16141) and *H. lepidus* (AMNH FM 143783), which display 2.04 (736°) and 2.2 (792°) cochlear turns, respectively (Table 6). The cochlear aspect ratio of *Ch. pelvidens* (NMMNH P-62258) is 0.53 (left bony labyrinth) and 0.54 (right bony labyrinth), which is similar to that of *D. ilicis* (AMNH VP 16141; 0.64) and *Protungulatum* sp. (AMNH VP 118359; 0.51) and contrasts with both specimens of *A. inopinata*, which exhibit flatter cochleae (0.40, MHNC 8399 and 0.48, MHNC 8360; Table 6). Overall, these values are lower compared with *H. lepidus* (AMNH FM 143783; 0.77) and *Ca. coarctatus* (AMNH 27601; 0.7). The basal and apical turns of the cochlear canals are not in contact in both the right and left bony labyrinths of *Ch. pelvidens* (NMMNH P-62258; Figs 7D and 9D), which is similar to the condition

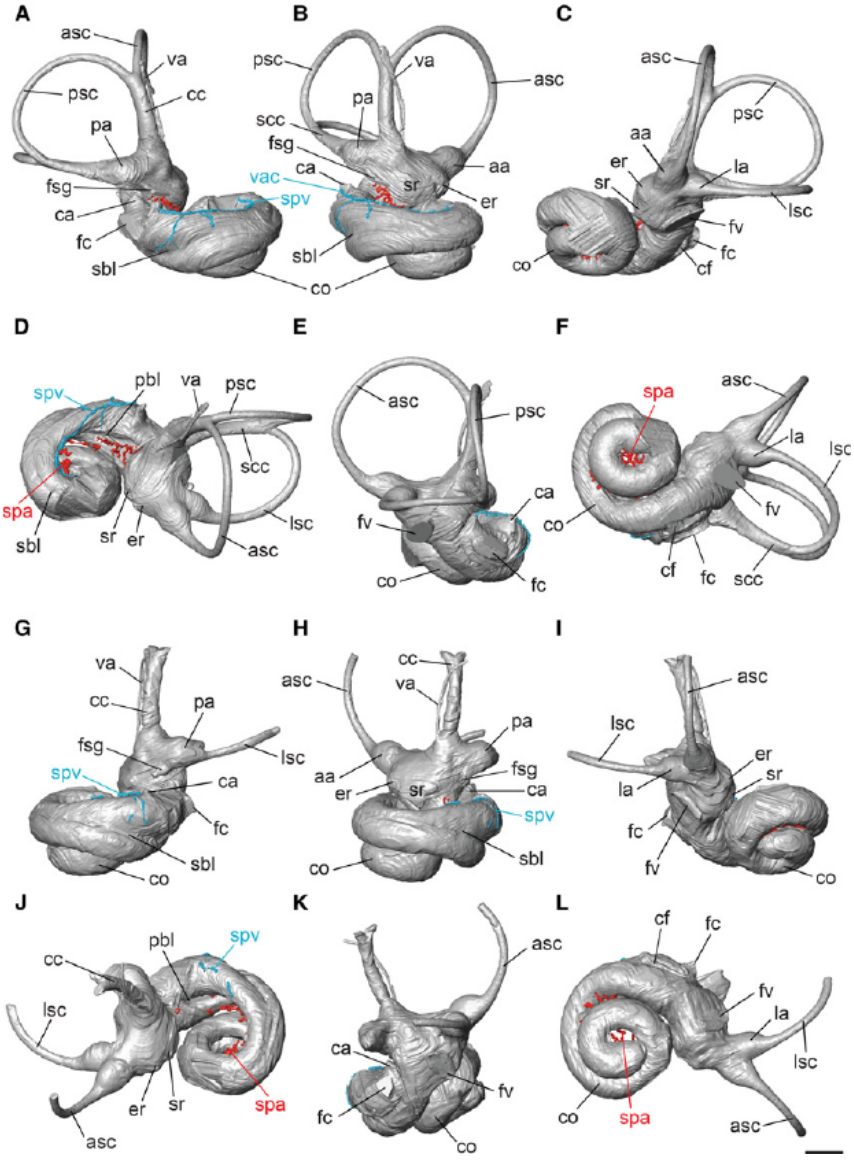

Fig. 7 Virtual endocasts of the left and right bony labyrinths of *Chriacus pelvidens* (NMMNH P-62258). (A,G) Posteromedial, (B, H) medial, (C,I) anterolateral, (D,J) dorsal, (E, K) posterolateral and (F,L) ventral views. Scale bar: 1 mm. aa, anterior ampulla; asc, anterior semicircular canal; ca, cochlear aqueduct; cc, common crus; cf, cochlear fossula; co, cochlear canal; er, elliptical recess; fc, fenestra cochleae; fsg, foramen singulare; fv, fenestra vestibuli; la, lateral ampulla; lsc, lateral semicircular canal; pa, posterior ampulla; pbl, primary bony lamina imprint; psc, posterior semicircular canal; sbl, secondary bony lamina imprint; scc, secondary common crus; spa, spiral modiolar artery; spv, spiral modiolar vein; sr, spherical recess; va, vestibular aqueduct; vac, vena aquaeductus cochleae. Veins are in blue and arteries in red.

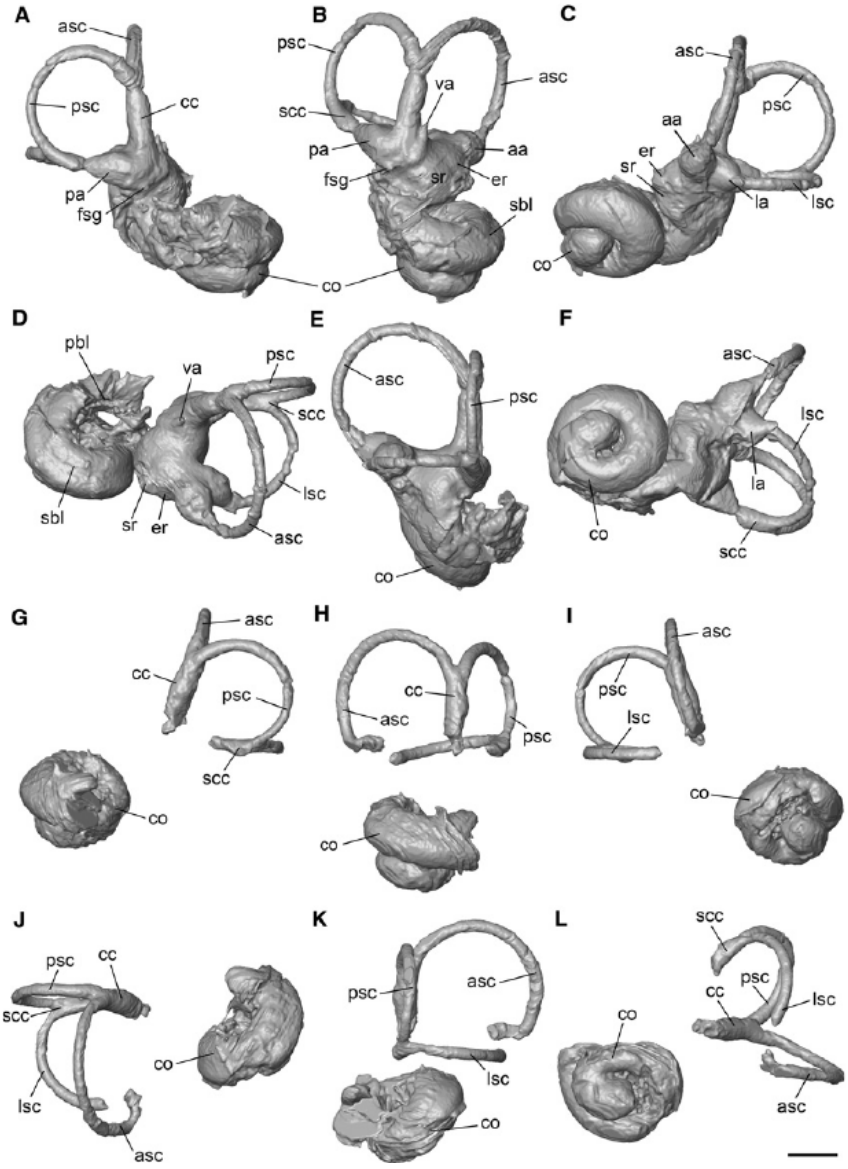

Fig. 8 Virtual endocasts of the left and right bony labyrinths of *Chriacus baldwini* (MCZ 20676). (A,G) Posteromedial, (B,H) medial, (C, I) anterolateral, (D,J) dorsal, (E,K) posterolateral and (F,L) ventral views. Scale bar: 1 mm. aa, anterior ampulla; asc, anterior semicircular canal; cc, common crus; co, cochlear canal; er, elliptical recess; fsg, foramen singulare; la, lateral ampulla; lsc, lateral semicircular canal; pa, posterior ampulla; pbl, primary bony lamina imprint; psc, posterior semicircular canal; sbl, secondary bony lamina imprint; scc, secondary common crus; sr, spherical recess; va, vestibular aqueduct.

in *Ca. coarctatus* (AMNH 27601; Fig. 9X), *A. inopinata* (MHNC 8399; Fig. 9T), *D. ilicis* (AMNH VP 16141) and *H. lepidus* (AMNH FM 143783; Fig. 9L). This condition contrasts with that of *Protungulatum* sp. (AMNH VP 118359), in which the turns of the cochlear canal are in contact (Fig. 9P). *Chriacus pelvidens* (NMMNH P-62258) has a stapedial ratio of 2.02, which is similar to that of *Protungulatum* sp. (AMNH VP 118359; 2.1) and the average value for the Cretaceous eutherian *Kulbeckia kulbecke* (2.0). All other specimens, including *D. ilicis* (AMNH VP 16141; 1.78) and *H. lepidus* (AMNH FM 143783; 1.44), have a stapedial ratio below 2.0 (see Table 6).

In life, the primary (inner) bony lamina and the secondary (outer) bony lamina would partially divide the scala tympani from the scala vestibuli of the cochlear canal (Meng & Fox, 1995). The scala tympani communicates with the fenestra cochleae, whereas the scala vestibuli connects to the fenestra vestibuli (Ekdale, 2016). These laminae are visible on the bony labyrinth endocast of *Ch. pelvidens* (NMMNH P-62258) and *Ch. baldwini* (MCZ 20676; Figs 7–9, Supporting Information Fig. S3). The secondary bony lamina is usually present among therians but might be absent in some cases (Meng & Fox, 1995; Ekdale, 2009). This bony lamina starts slightly before the fenestra cochleae, as illustrated by Ekdale (2009: fig. 4.1a) and extends far into the canal beyond the first half of the basal turn until 380.7° of this turn, and represents 57% of the total cochlear coil in NMMNH P-62258. The basal part of the cochlea is not preserved well enough in the left bony labyrinth of MCZ 20676 to obtain a measure of the secondary bony lamina; however, the secondary bony lamina visibly extends even farther into the canal of this specimen, suggesting the measurement found for in NMMNH P-62258 can be considered a minimum. The secondary bony lamina also extends far into the canal in *Protungulatum* sp. (AMNH VP 118359; 340°, 61%) in a similar fashion to MCZ 20676 (Fig. 9P). This

Table 6 Measurements of 3D reconstructions from CT data of the endocasts of the bony labyrinth of *Chriacus pelvidens* (NMMNH P-62258) and *Chriacus baldwini* (MCZ 20676). Comparisons with other early placental mammals and Cretaceous eutherians.

	Ch. baldwini (MCZ 20676; Left ear)	*Ch. pelvidens* (NMMNH P-62258; Left ear)	*Ch. pelvidens* (NMMNH P-62258; Right ear)	*Diacodexis ilicis* (AMNH VP 16141)	*Hyopsodus lepidus* (AMNH FM 143783)	*Protungulatum* sp. (AMNH VP 118359)	*Alcidedorbignya inopinata* (MHNC 8399)	*Alcidedorbignya inopinata* (MHNC 8360)	*Carsioptychus coarctatus* (AMNH 27601)	*Ukhaatherium gobiensis* (PSS-MAE 110)	*Kulbeckia kulbecke*	*Zalambdalestes lechei*	zhelestids
Stapedial aspect ratio	–	2.02	–	1.78	1.44	2.1	1.8	1.7	–	1.5	2.0	1.7	1.6
Cochlear aspect ratio	–	0.53	0.54	0.64	0.77	0.51	0.40	0.48	0.70	0.35	0.44	0.36	0.46
Cochlear coil (°)	–	–	672.3	736	792	553	540	540	600	380	446	368	545
Number of cochlear turns	–	–	1.87	2.04	2.20	1.54	1.50	1.50	1.67	1.06	1.24	1.02	1.51
Cochlear canal length (mm)	–	–	12.33	7.35	10.10	7.10	10.86	8.48	9.27	2.77	4.93	3.40	4.93
Secondary lamina coil (°)	–	–	380.7	180	135	340	90	90	130	76.8	209	95.3	198
Secondary lamina coil (%)	–	–	57	24	17	61	17	17	22	20	47	26	36
Basal turn/LSC angle (°)	24.8	29.6	31.8	13	20	–	35.86	23.11	29	6.63	12.1	13.5	34°
Total labyrinth volume (mm^3)	–	16.92	–	11.77	11.5	5.10	–	–	–	2.17	5.37	6.07	6.28
Cochlear volume (mm^3)	–	10.55	10.39	6.53	7.19	3.10	–	–	7.25	1.23	2.59	2.91	4.15
Cochlear volume/ total volume (%)	–	62.3	–	55.5	62.5	60.8	[a]50	–	56.7	48.2	47.9	66.1	
Angle ASC/LSC (°)	83	85.8	–	73	91.5	74	83.71	87.08	80	88.8	79.9	81.0	88.8
Angle LSC/PSC (°)	92.5	88.6	–	81	91	98	90.33	90.59	80	88.4	89.6	85.6	93.1
Angle ASC/PSC (°)	95.8	93.5	–	95	84	81	90.1	69.4	90	105	79.9	93.6	96.8
ASC H/W (mm)	2.48/2.49	3.51/3.62	–	3.49/3.36	3.12/2.81	2.46/2.27	2.25/2.26	2.27/2.0	3.48/3.61	–	–	–	–
ASC R/L (mm)	1.24/6.13	1.78/8.50	–	1.71/8.69	1.48/7.2	1.18/5.97	1.13/7.42	1.07/7.21	1.77/7.90	0.84/3.81	1.19/5.70	1.46/6.92	1.17/5.80
PSC H/W (mm)	2.25/2.12	3.39/3.26	–	2.39/3.09	2.43/2.36	2.16/1.94	2.01/2.03	–	3.74/3.19	–	–	–	–
PSC R/L (mm)	1.09/5.36	1.66/8.85	–	1.37/7.68	1.19/7.1	1.02/5.79	1.01/6.51	–	1.73/9.58	0.69/3.39	0.96/4.55	1.20/5.85	0.86/4.62
LSC H/W (mm)	1.54/2.03	2.75/2.58	–	2.17/2.79	2.34/2.14	1.95/1.82	2.05/2.06	1.77/1.79	3.88/3.02	–	–	–	–
LSC R/L (mm)	0.89/3.28	1.33/5.79	–	1.24/5.05	1.12/5.34	0.94/4.23	1.03/6.80	0.89/5.81	1.73/7.33	0.74/3.16	0.92/3.94	1.21/5.20	0.79/3.49
ratio ASC H/W (mm)	1.0	1.0	–	1.0	1.1	1.1	1.0	1.1	1.0	–	–	–	–
ratio PSC H/W (mm)	1.1	1.0	–	0.8	1.0	1.1	1.0	–	1.2	–	–	–	–
ratio LSC H/W (mm)	0.8	1.1	–	0.8	1.1	1.1	1.0	1.0	1.3	–	–	–	–

ASC, anterior semicircular canal; H, height; L, length; LSC, lateral semicircular canal; PSC, posterior semicircular canal; R, radius; W, width.

[a]The cochlear volume/total volume for *Alcidedorbignya inopinata* is based on MHNC 8360 and MHNC 8359 (Muizon et al., 2015). Number of turns was determined based on the cochlear coiling/360° (Ekdale, 2009). Data for zhelestids, *Kulbeckia kulbecke* and *Zalambdalestes lechei* are averages based on several specimens from Ekdale & Rowe (2011). The data for *Ukhaatherium gobiensis* are from Ekdale (2013). Data for *Protungulatum* sp. (AMNH VP 118359), *Hyopsodus lepidus* (AMNH FM 143783) and *Diacodexis ilicis* (AMNH VP 16141) are from Orliac & O'Leary (2016); data for *Carsioptychus coarctatus* (AMNH 27601) are from Cameron et al. (2019).

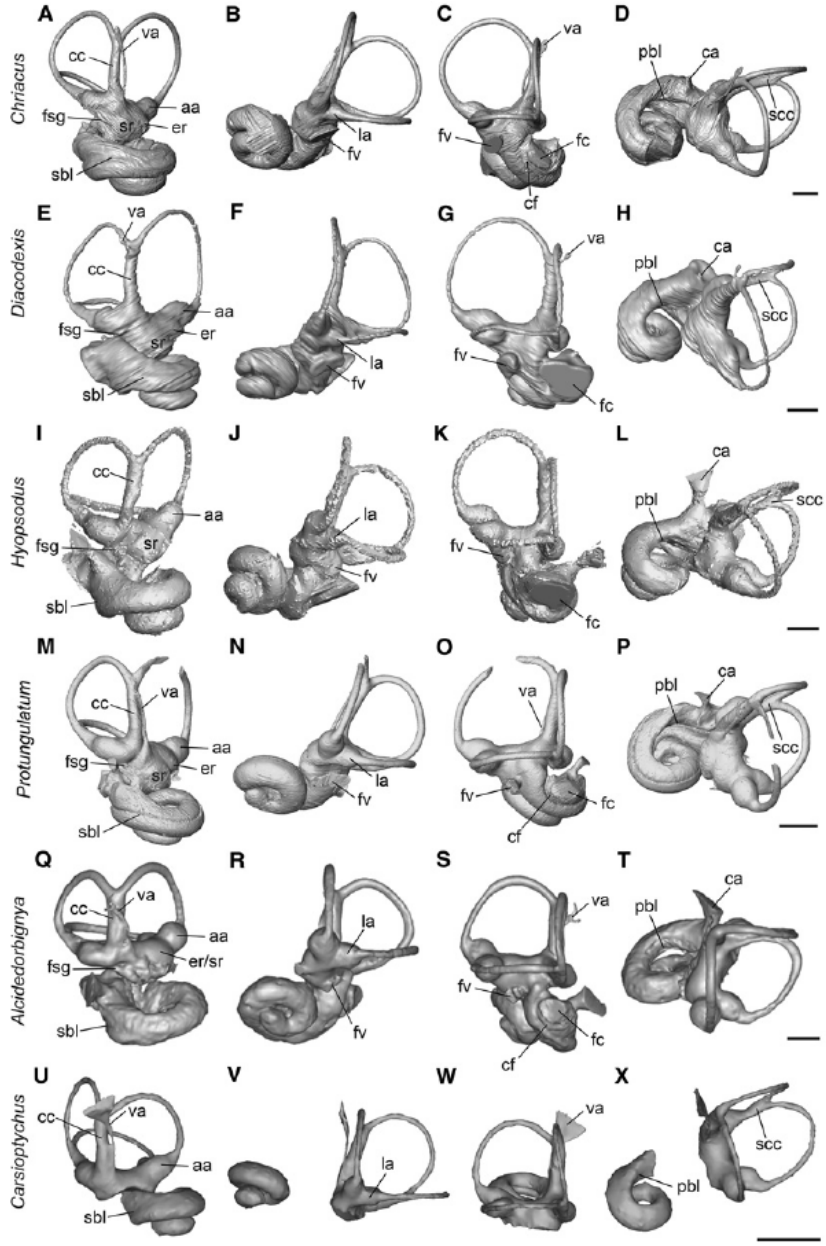

Fig. 9 Comparison of the bony labyrinth morphology of *Chriacus pelvidens* (NMMNH P-62258) with other early placental mammals. Taxa illustrated are (A–D) *Ch. pelvidens* (NMMNH P-62258); (E–H) *Diacodexis ilicis* (AMNHVP 16141; Orliac et al., 2012b); (I–L) *Hyopsodus lepidus* (AMNHFM 143783; Ravel & Orliac, 2015); (M–P) *Protungulatum* sp. (AMNHVP 118359; Orliac & O'Leary, 2016); (Q–T) *Alcidedorbignya inopinata* (MHNC 8399; Muizon et al., 2015); (U–X) *Carsioptychus coarctatus* (AMNH 27601; Cameron et al., 2019). Scale bars: 1 mm. (A, E, I, M, Q, U) Medial, (B, F, J, N, R, V) anterolateral, (C, G, K, O, S, W) posterolateral and (D, H, L, P, T, X) dorsal views. aa, anterior ampulla; ca, cochlear aqueduct; cc, common crus; cf, cochlear fossula; er, elliptical recess; fc, fenestra cochleae; fsg, foramen singulare; fv, fenestra vestibuli; la, lateral ampulla; pbl, primary bony lamina imprint; psc, posterior semicircular canal; sbl, secondary bony lamina imprint; scc, secondary common crus; sr, spherical recess; va, vestibular aqueduct. All the specimens are left inner ears except *A. inopinata* (MHNC 8399), which is a mirrored image of the right inner ear.

contrasts with other compared specimens, which show less expansion of the secondary lamina coil (Table 6). The primary bony lamina is also visible in *Ch. pelvidens* (NMMNH P-62258 and MCZ 20676), *Protungulatum* sp. (AMNH VP 118359), *H. lepidus* (AMNH FM 143783), *A. inopinata* (MHNC 8399) and *D. ilicis* (AMNH VP 16141; Fig. 9). The lamina gap between the primary and the secondary bony laminae becomes progressively wider and then narrower towards the apex in *Ch. pelvidens* (NMMNH P-62258), which contrasts with the condition of *Protungulatum* sp. (AMNH VP 118359), *A. inopinata* (MHNC 8399; MHNC 8360) and Cretaceous eutherians, which have a wider lamina gap closer to the apex (see Ekdale & Rowe, 2011: fig. 5; Orliac & O'Leary, 2016). Nevertheless, caution should be used when interpreting lamina gap measurements because the state of preservation of the primary bony lamina in *Ch. pelvidens* (NMMNH P-62258) is incomplete along the cochlear canal. As the bony labyrinth of *Ch. baldwini* (MCZ 20676) is filled with a white dense material, it is not possible to identify the lamina gap in the CT data of this specimen. This measurement was not recorded for *D. ilicis* (AMNH VP 16141) or *H. lepidus* (AMNH FM 143783).

The aperture of the cochlear fossula leading to the fenestra cochleae (e.g. MacPhee, 1981; Wible et al., 2007, 2009; Billet & Muizon, 2013; Muizon et al., 2015) and the cochlear fossula are visible on the bony labyrinth endocast in *Ch. pelvidens* (NMMNH P-62258; Fig. 9C), as in *Protungulatum* sp. (AMNH VP 118359; Fig. 9O; Orliac & O'Leary, 2016: fig. 2f), *A. inopinata* (MHNC 8399; Fig. 9S; Muizon et al., 2015: fig. 52b), an early notoungulate MNHN-F-BRD 23 (Billet & Muizon, 2013: fig. 5b) and a litoptern UFRJ-DG 119-M (Billet et al., 2015: fig. 7c). Neither feature could be

identified in *D. ilicis* (AMNH VP 16141; Orliac et al., 2012a: fig. 2e) and *H. lepidus* (AMNH FM 143783; Ravel & Orliac, 2015: fig. 2d); therefore, we annotated this region, the fenestra cochleae, for both specimens (Fig. 9G,K). The cochlear fossula is also not visible on bony labyrinth endocasts in Cretaceous eutherians (Ekdale, 2009; Ekdale & Rowe, 2011: figs, 3b, 6c). However, as noted by Orliac & O'Leary (2016), better-preserved specimens would be required to confirm their absence in *D. ilicis* and *H. lepidus*. The fenestra cochleae in *Protungulatum* sp. (AMNH VP 118359; Fig. 9O), *D. ilicis* (AMNH VP 16141; Fig. 9G) and *H. lepidus* (AMNH FM 143783; Fig. 9K) extends posteriorly beyond the posterior semicircular canal (PSC), similar to the fenestra cochleae of *Ch. pelvidens* (NMMNH P-62258; Fig. 9C). This contrasts with the condition of *A. inopinata* (MHNC 8399; Fig. 9S), in which the fenestra cochleae does not extend posteriorly beyond the PSC. The horseshoe-shaped outpocketing of the cochlear fossula, which is lateral to the base of the cochlear aqueduct in *Protungulatum* sp. (AMNH VP 118359; Supporting Information Fig. S4D) and litoptern indet. (UFRJ-DG 119-M; Fig. S4E), is absent in *Ch. pelvidens* (NMMNH P-62258; Fig. S4A), *D. ilicis* (AMNH VP 16141; Fig. S4B) and *H. lepidus* (AMNH FM 143783; Fig. S4C). This feature could not be determined in *A. inopinata* (MHNC 8399). However as previously mentioned, this could be related to limited preservation of this region in *D. ilicis*, *H. lepidus* (Orliac & O'Leary, 2016) and *Ch. pelvidens*. These different features could not be identified for the bony labyrinths of *Ch. baldwini* (MCZ 20676) because of the lack of preservation of this region (Fig. 8).

The cochlea represents a higher volume percentage compared with the vestibular apparatus portion in *Ch. pelvidens* (NMMNH P-62258; 62.3%), *H. lepidus* (AMNH FM 143783; 62.5%), *Protungulatum* sp. (AMNH VP 118359; 60.8%) and *D. ilicis* (AMNH VP 16141; 55.5%), whereas the two are approximately equal in *A. inopinata* (MHNC 8399; MHNC 8360; 45–50%). Cretaceous eutherians cover the range of variation for cochlear volume percentage of placental mammals from our sample (47.9–66.1%; Table 6). This measure was not obtained for *Ch. baldwini* (MCZ 20676) because of the incompleteness of the cochleae on both sides (Fig. 8).

Vestibule

The vestibular apparatus of *Ch. pelvidens* (NMMNH P-62258) and *Ch. baldwini* (MCZ 20676) is similar in overall morphology to that of other early placental mammals and close relatives: *Protungulatum* sp. (AMNH VP 118359), *D. ilicis* (AMNH VP 16141), *H. lepidus* (AMNH FM 143783), *A. inopinata* (MHNC 8399; MHNC 8360), litopterns (UFRJ-DG 119-M), *Ca. coarctatus* (AMNH 27601) and Cretaceous eutherians (Ekdale & Rowe, 2011). All the aforementioned specimens, including *Ch. pelvidens* (NMMNH P-62258) and *Ch. baldwini* (MCZ 20676), have a second common crus (Fig. 9). The vestibular aqueduct bony channel is visibly better preserved in *Ch. pelvidens* NMMNH P-62258 (Fig. 7B) than in *Ch. baldwini* (MCZ 20676), in which only the root of the vestibular aqueduct can be identified (Fig. 8B). In *Ch. pelvidens* (NMMNH P-62258) and in *Ch. baldwini* (MCZ 20676) the root of the vestibular aqueduct starts next to the base of the common crus, close to the posterior ampulla (Figs 7B and 8B), and this is similar to the condition of *Protungulatum* sp. (AMNH VP 118359; Fig. 9M) and the litoptern UFRJ-DG 119-M (Orliac & O'Leary, 2016: fig.3l). *Chriacus baldwini* (MCZ 20676) exhibits a bulge at the base of the vestibular aqueduct (Fig. 8B) as in *Protungulatum* sp. (AMNH VP 118359; Fig. 9M) and the litoptern UFRJ-DG 119-M (Orliac & O'Leary, 2016: fig.3l). This area is not preserved well enough in *Ch. pelvidens* (NMMNH P-62258; Fig. 7B). This contrasts with *Ca. coarctatus* (AMNH 27601; Fig. 9U), *A. inopinata* (MHNC 8399; Fig. 9Q) and *D. ilicis* (AMNH VP 16141; Fig. 9E), in which the vestibular aqueduct starts higher on the common crus.

The passageway for the inferior vestibular nerves corresponds to the foramen singulare, which is ventral to the posterior ampulla (Wible et al., 2008, 2010; Billet & Muizon, 2013; Muizon et al., 2015; Orliac & O'Leary, 2016). This foramen is visible in both bony labyrinths of *Ch. pelvidens* (NMMNH P-62258; Fig. 9A) and in *Ch. baldwini* (MCZ 20676; Fig. 8b), *Protungulatum* sp. (AMNH VP 118359; Fig. 9M), *D. ilicis* (AMNH VP 16141; Fig. 9E), *H. lepidus* (AMNH FM 143783; Fig. 9I) and *A. inopinata* (MHNC 8399; Fig. 9Q).

The elliptical (membranous utricle) and spherical (membranous saccule) recesses form two distinct swellings ventral to the anterior ampulla in *Ch. pelvidens* (NMMNH P-62258; Fig. 9A), and *Ch. baldwini* (MCZ 20676; Fig. 8B), which is similar to that of *Protungulatum* sp. (AMNH VP 118359; Fig. 9M) and *D. ilicis* (AMNH VP 16141; Fig. 9E), but is less pronounced in *H. lepidus* (AMNH FM 143783; Fig. 9I). The distinction between these two structures could not be identified in *Ca. coarctatus* (AMNH 27601), litopterns (e.g. UFRJ-DG 1035-M) or *A. inopinata* (MHNC 8399; MHNC 8360) and are probably housed in a common chamber. Finally, the fenestra cochleae is positioned posteromedial to the fenestra vestibuli and is directed laterally relative to the PSC in all specimens (Fig. 9). The fenestrae cochleae and vestibuli are not preserved in *Ch. baldwini* (MCZ 20676; Fig. 8).

Semicircular canals

Measurements of the semicircular canals are presented in Tables 6 and S4. The semicircular canals are complete in the left bony labyrinth, but not in the right bony labyrinth, of NMMNH P-62258 (Fig. 7) and in MCZ 20676 (Fig. 8). The angle between the lateral semicircular canal (LSC) and the basal turn of the cochlea is higher in *Ch. pelvidens* (NMMNH P-62258; ~30°), *Ch. baldwini* (MCZ 20676; ~ 25°), *Ca. coarctatus* (AMNH 27601; 29°) and zhelestids (average value of 34°) than in *A. inopinata* (MHNC 8399, 35.9°; MHNC 8360; 23.1°), *D. ilicis* (AMNH VP 16141; 13°),

H. lepidus (AMNH FM 143783; 20°) or various Cretaceous eutherians (Table 6). The widest angle is between the anterior (ASC) and posterior (PSC) semicircular canals in *Ch. pelvidens* (NMMNH P-62258; 93.5°) and in *Ch. baldwini* (MCZ 20676; 95.8°), which is similar to *D. ilicis* (AMNH VP 16141; 95°), *Ca. coarctatus* (AMNH 27601; 90°) and Cretaceous eutherians except *Kulbeckia kulbecke* (Ekdale & Rowe, 2011; 93;.6°–105°). In other taxa, the widest angle can be between the lateral (LSC) and posterior (PSC) canals (e.g. *Protungulatum* sp., AMNH VP 118359) or between the LSC and the PSC, as well as the ASC and the LSC (*H. lepidus*; AMNH FM 143783). There is more variation in terms of the shortest angle between canals in our sample. The shortest angle is between the ASC and the LSC in *Ch. pelvidens* (NMMNH P-62258; 85.8°) and in *Ch. baldwini* (MCZ 20676; 83°), which is similar to that of *D. ilicis* (AMNH VP 16141; 73°), *Protungulatum* sp. (AMNH VP 118359; 74°), *A. inopinata* (MHNC 8399; 83.7°), *Zalambdalestes lechei* (81.0°) and zhelestids (Ekdale & Rowe, 2011; 88;.8°). In other taxa, the shortest angle is between the ASC and the LSC, as well as the LSC and the PSC (e.g. *Carsioptychus coarctatus*, AMNH 27601; Table 6), between the ASC and the PSC (i.e. *A. inopinata*, MHNC 8360) and between the ASC and the LSC, as well as the ASC and the PSC (i.e. *Kulbeckia kulbecke*; Ekdale & Rowe, 2011).

Of the three canals, the ASC has the largest radius in *Ch. pelvidens* (NMMNH P-62258) and in *Ch. baldwini* (MCZ 20676), which is similar to all other early placental mammals and Cretaceous eutherians (Table 6). The canal with the shortest radius is the LSC in *Ch. pelvidens* (NMMNH P-62258), *Ch. baldwini* (MCZ 20676), *Protungulatum* sp. (AMNH VP 118359), *D. ilicis* (AMNH VP 16141), *H. lepidus* (AMNH FM 143783) and all Cretaceous eutherians (Table 6). This contrasts with *A. inopinata* (MHNC 8399) and *Ca. coarctatus* (AMNH 27601), in which the shortest radii are for the LSC and the PSC. In terms of length, the PSC is the longest canal for *Ch. pelvidens* (NMMNH P-62258), as in *Ca. coarctatus* (AMNH 27601), which differs from *Ch. baldwini* (MCZ 20676) and other early placental mammals and Cretaceous eutherians, which have the ASC as the longest canal (Table 6). The shortest canal is the LSC for *Ch. pelvidens* (NMMNH P-62258), *Ch. baldwini* (MCZ 20676), all other early placental mammals and Cretaceous eutherians except *A. inopinata* (MHNC 8399), in which the PSC is the shortest canal (Table 6).

The ratios between the height and width of the canals are close to 1 in *Ch. pelvidens* (NMMNH P-62258) and in *A. inopinata* (MHNC 8399). *Chriacus baldwini* (MCZ 20676) displays a similar condition, but its LSC dimensions deviate slightly from the above taxa, with a ratio of 0.8. In general, the ratios of the height vs. width for the different canals in all specimens are around 1.0–1.1. Only *D. ilicis* (AMNH VP 16141; ratio of 0.8 [PSC and LSC)]) and *Ca. coarctatus* (AMNH 27601; ratio of 1.2 [PSC] and 1.3 [LSC]) show a deviation from this observation for the PSC and the LSC. The height and width ratio of the ASC is consistently close to 1.0–1.1 in all specimens (Table 6).

Blood vessels

Blood vessels, including veins and arteries, can be identified in both bony labyrinths of *Ch. pelvidens* (NMMNH P-62258; Fig. 7) but not *Ch. baldwini* (MCZ 20676; Fig. 8). The labyrinthine artery is a branch of the anterior inferior cerebellar artery that provides blood supply to the cochlea (Gray, 1918). Inside the mammalian cochlea, the spiral modiolar artery distributes the blood (Axelsson & Ryan, 1988). In *Ch. pelvidens* (NMMNH P-62258), the cast for the spiral modiolar artery as well as its arterioles are visible, departing from the base to the apex of the cochlea around the modiolus (Figs 7 and S3). A similar, or even finer, level of preservation is seen in *Protungulatum* sp. (AMNH VP 118359; see Orliac & O'Leary, 2016: fig. 2d). The cast of the spiral modiolar vein is also visible in *Ch. pelvidens* (NMMNH P-62258; Figs 7D, S3); however, it is not as well preserved as in *Protungulatum* sp. (AMNH VP 118359; Orliac & O'Leary, 2016: fig. 2d) or in *Diplobune minor* (UM ITD 1081; Orliac et al., 2017: fig. 7c,d). The vena aquaeductus cochleae is visible in *Ch. pelvidens* (NMMNH P-62258; Fig. 7B). Venules radiating from the spiral modiolar vein are present on the basal turn of the cochlear canal (Fig. 7D). In life, the spiral modiolar vein drained into the vena aquaeductus cochleae (Axelsson & Ryan, 1988). As in *Protungulatum* sp. (AMNH VP 118359; Orliac & O'Leary, 2016; : fig. 2d) and in *Diplobune minor* (UM ITD 1081; Orliac et al., 2017: fig. 7c), the vena aquaeductus cochleae is a separate canal from the cochlear aqueduct in *Ch. pelvidens* (see Fig. 7B). The structure of the vessels is similar in zhelestids (Ekdale & Rowe, 2011).

Quantitative analyses

Hearing range

Three different equations were used to determine the hearing range of *Ch. pelvidens* (see Table 1). The hearing frequency range of our specimen (NMMNH P-62258) is between 0.32 and 40.29 kHz with the equation from West (1985), 0.64–40.26 with Rosowski (1992), and 0.64–46.22 with Rosowski & Graybeal (1991) and Rosowski (1992). We visually compared the hearing frequency of *Ch. pelvidens*, calculated using the equation from West (1985), with that of other extant and extinct taxa (see Fig. 10; Table S5). *Chriacus pelvidens* had a hearing frequency range close to that of the extant aardvark (*Orycteropus afer*) and nine-banded armadillo (*Dasypus novemcinctus*) as well as that of the fossil taxon *H. lepidus* (AMNH 143783; see Fig. 10). *Chriacus pelvidens* (NMMNH P-62258) and *H. lepidus* (AMNH FM 143783) had very similar low frequency hearing limits: 0.32 and 0.33, respectively. However, *H. lepidus* (AMNH FM 143783) was able to hear higher frequency sounds compared with our specimen of *Ch. pelvidens* (Table S5;

Fig. 10). *Chriacus pelvidens* (NMMNH P-62258) also had a lower high-frequency hearing limit compared with both the potential stem euungulate *Protungulatum* sp. (AMNH VP 118359) and the early artiodactyl *D. ilicis* (AMNH VP 16141), as well as *A. inopinata* (MHNC 8360), *Ca. coarctatus* (AMNH 27601) and Cretaceous eutherians (Table S5; Fig. 10). *Chriacus pelvidens* also had a range of hearing in octaves (7.0) close to those of the large slit-faced bat (*Nycteris grandis*; 7.05) and the Virginia opossum (*Didelphis virginiana*; 7.15; see Table S5; Fig. 10).

Locomotor agility

Agility scores (AS) were obtained for *Ch. pelvidens* (NMMNH P-62258) and *Ch. baldwini* (MCZ 20676) based on the equations from Silcox et al. (2009a). *Chriacus pelvidens* (NMMNH P-62258) and *Ch. baldwini* (MCZ 20676) had average agility scores between 2.62 and 3.45, and 2.09–2.86, respectively, depending on the canal and body mass measures (BM) used in the equation (Tables 2 and S4). This suggests that *Ch. pelvidens* (NMMNH P-62258) and *Ch. baldwini* (MCZ 20676) were slow-to-medium moving mammals. Using the semicircular canal average (SC), *Ch. pelvidens* (NMMNH P-62258) overlaps with *A. inopinata* (MHNC 8399), and *Ch. baldwini* (MCZ 20676) overlaps with *Ca. coarctatus* (AMNH 27601; Fig. 11). Extant mammals (data from Spoor et al., 2007) that have similar agility scores for the highest body mass range of *Ch. pelvidens* (NMMNH P-62258) are, for example, the American badger (*Taxidea taxus*, BM = 7190 g; AS = 3) and the crab-eating raccoon (*Procyon cancrivorus*, BM = 6994 g; AS = 3). This result contrasts with the agility scores obtained with the lowest body mass estimate for *Ch. pelvidens* (NMMNH P-62258). In this scenario, *Ch. pelvidens* (NMMNH P-62258) is in the

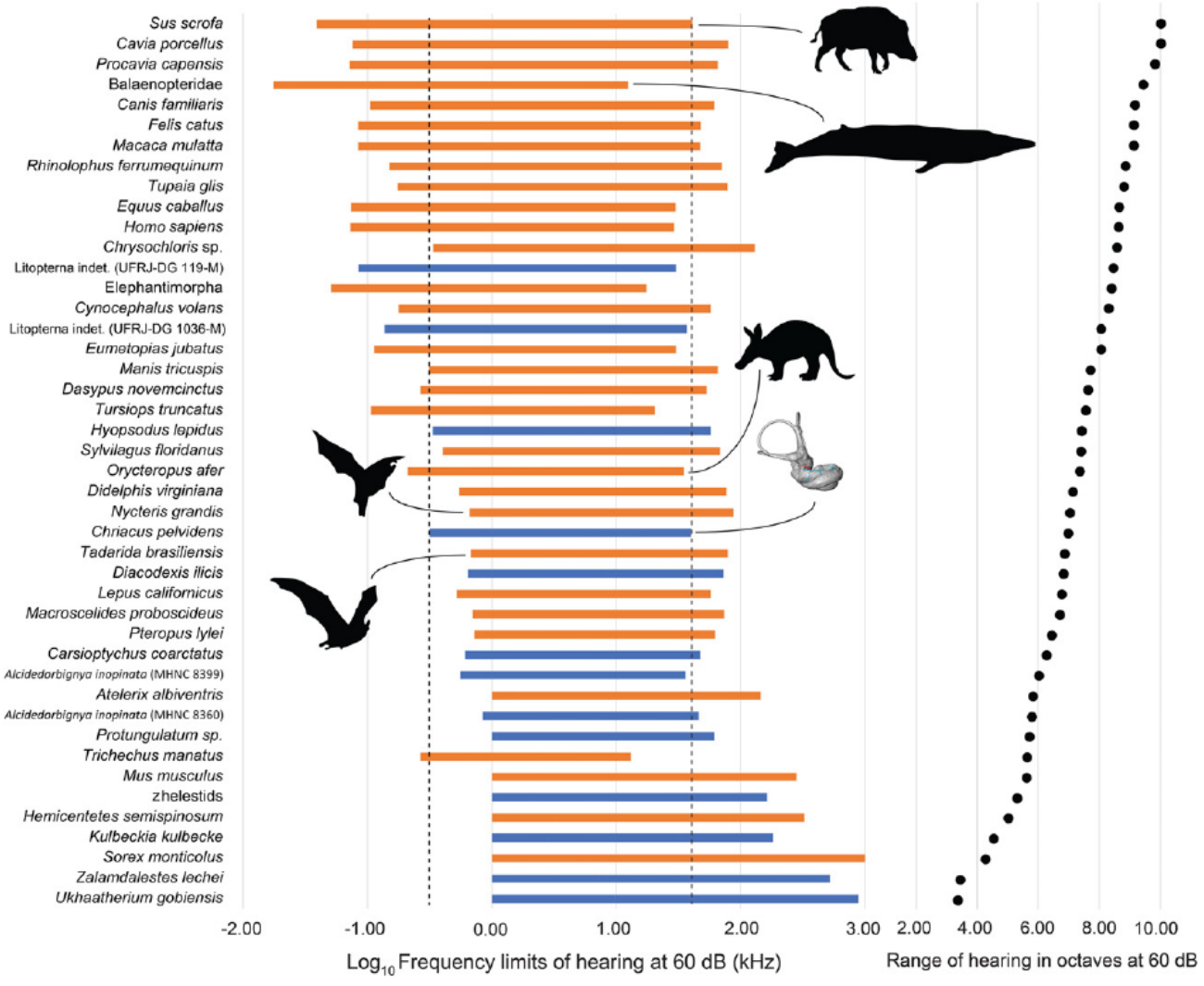

Fig. 10 Log_{10} of the frequency limits of hearing at 60 dB (kHz) and the corresponding range of hearing in octaves of *Chriacus pelvidens* (NMMNH P-62258), extant and extinct mammals. Data are from Table S5.

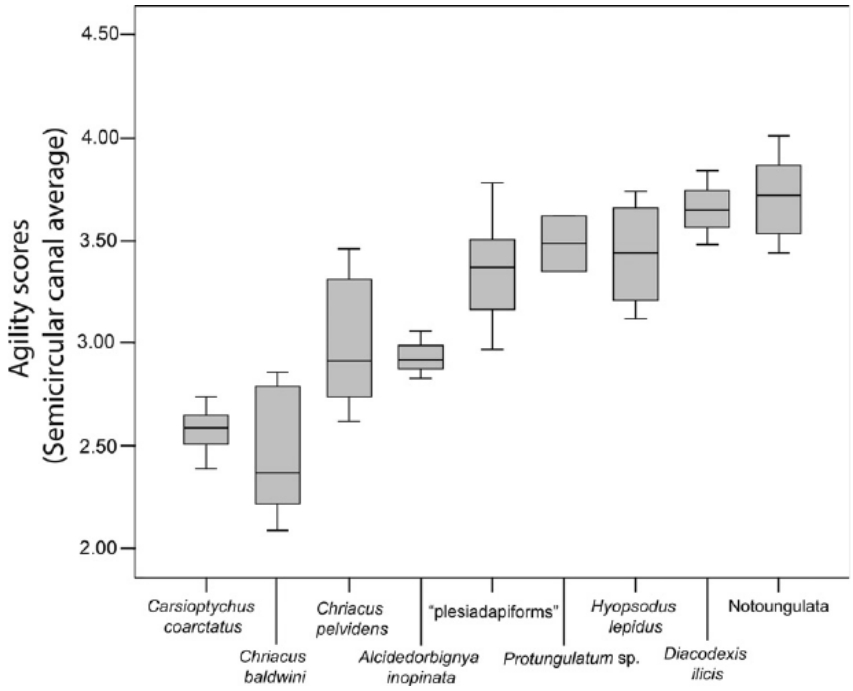

Fig. 11 Agility score boxplot based on the semicircular canal averages of *Chriacus pelvidens* (NMMNH P-62258), *Chriacus baldwini* (MCZ 20676) and selected Paleocene-Eocene placental mammals. Data are from Table S4.

range of *Protungulatum* sp. (AMNH VP 118359), *H. lepidus* (AMNH FM 143783) and *D. ilicis* (AMNH VP 16141), as well as plesiadapiform primates (Silcox et al., 2009a; Fig. 11). Compared with extant taxa (data from Spoor et al., 2007), this means that *Ch. pelvidens* (NMMNH P-62258) would have had an agility closer to that of mammals such as the dwarf armadillo (*Zaedyus pichiy*, BM = 1740 g; AS = 3). On the basis of the average body mass, *Ch. pelvidens* would have had an agility closer to that of the raccoon dog (*Nyctereutes procyonoides viverrinus*, BM = 4500 g; AS = 3). For *Ch. baldwini* (MCZ 20676), extant mammals of similar body mass estimates with similar agility scores are the northern common cuscus (*Phalenger orientalis,* BM = 2500 g; AS = 2) and the crested rat (*Lophiomysimhausi,* BM = 755 g; AS = 2). The agility score of *Ch. baldwini* (MCZ 20676) is lower than those of extant artiodactyls of similar body masses, such as the water deer (*Hydropotes inermis*, BM = 1285 g) and Java mouse-deer (*Tragulus javanicus*, BM = 2000 g), which are 4 (Cox & Jeffery, 2010).

Brain size and EQ

The endocranial volume of *Ch. baldwini* (MCZ 20676) is 2699 mm^3 (Table 3). Based on Eisenberg's (1981) equation, the EQ of *Ch. baldwini* (MCZ 20676) is between 0.12 and 0.41, depending on which body mass value is used (Table 2). This is higher than the range of values obtained for *O. tisonensis* (AMNH 785; 0.08–0.10) and lower than the EQ of *D. ilicis* (AMNH VP 16141; 0.54–0.79), but overlaps with *A. inopinata* (MHNC 8372; 0.36–0.49) and is in the low range of EQ variation of *H. lepidus* (AMNH FM 143783; 0.34–0.70; Table 3). Cameron et al. (2019) hypothesized that Paleocene 'archaic' placentals may have had abnormally low EQ values compared with extant placentals, and perhaps even to their Mesozoic antecedents. The low EQ results for *Ch. baldwini* are consistent with this hypothesis, which remains to be tested statistically with a much larger sample. This will be the subject of future work from our research group.

Discussion

The senses and behavior of *Chriacus*

Based on the available data, *Ch. baldwini* probably relied heavily on its sense of smell, compared with the other major senses that we are able to study. Regarding vision, both the petrosal lobules and the visual cortex contribute to this sense. Of these, only the petrosal lobules can be identified in both *Ch. pelvidens* and *Ch. baldwini*. These cerebellar structures play a role in the control of eye movements, also known as vestibulo-ocular reflex (VOR; Rambold et al., 2002). Large petrosal lobules are present in more active and visually oriented animals, such as arboreal squirrels, compared with more slow-moving and fossorial taxa like the mountain beaver (*Aplodontia rufa*; Bertrand et al., 2017, 2018b). The average petrosal volume percentage is 0.96%, with a range of 0.01–2.34%, for 49 species of mammals (Ferreira-Cardoso et al., 2017) and 1.78%, with a range of 0.39–3.35%, for 33 Ischyromyidae and Sciuroidea rodent species (Bertrand et al., 2018b). This suggests that the petrosal lobules of *Ch. baldwini* can be considered small (0.26% of brain volume) and thus that this species probably had a

lower vestibulo-ocular reflex compared with those of more active and visually oriented mammals.

The visual cortex localized in the occipital lobe of the neocortex (Martin, 1990) also contributes to vision. An expanded neocortex has been associated with improved vision in primates and rodents because the posterior region of this structure, where the visual cortex is located, is expanded and covers the midbrain (Silcox et al., 2010; Bertrand et al., 2018b). Because this region of the brain is not preserved in *Ch. baldwini,* it is impossible to determine with certitude whether the cerebrum was covering the midbrain. However, thus far, no fossil mammals from the Mesozoic or Paleocene have been found with an expanded cerebrum covering the midbrain (Edinger, 1964; Silcox et al., 2011; Muizon et al., 2015), so it seems unlikely that *Ch. baldwini* would have had this condition.

Concerning olfaction, the average olfactory bulb volume percentage is 3.47% (range: 1.64–6.05%) for 33 Ischyromyidae and Sciuroidea rodent species (Bertrand et al., 2018b), and 1.38% (range: 0.01–7.80%) for 51 species of primates (i.e. plesiadapiforms and euprimates; gathered from the literature by Bertrand et al., 2017). Therefore, the olfactory bulbs of *Ch. baldwini* can be considered large (6.9%) when compared with the olfactory bulbs of those taxa, and suggest a high reliance on olfaction.

Chriacus pelvidens was able to hear the same range of high frequencies as the extant aardvark and the nine-banded armadillo; however, both extant species can hear lower frequency sounds compared with what *Ch. pelvidens* likely was capable of hearing. Moreover, the armadillo and *H. lepidus* have a higher frequency hearing limit compared with that of *Chriacus*.

Early Paleocene mammals filled many different niches, similar to their Mesozoic ancestors (Luo, 2007), but differed in that they had a much larger range of body sizes; particularly, there were much larger species than before the end-Cretaceous mass extinction (Alroy, 1999; Slater, 2013). Locomotor behaviors are best reconstructed for fossil taxa using postcranial elements, when available (e.g. Carrano, 1999; Chester et al., 2017). A large amount of postcranial fossils have been described for *Chriacus*, including postcrania of *Ch. baldwini* and *Ch. gallinae* by Matthew (1897, 1915) and postcrania of *Ch. orthogonius* by Szalay & Lucas (1996). Rose (1987) described the most complete skeleton of *Chriacus* but because no teeth were found in association, it could not be identified to the species level and was referred to as *Chriacus* sp. Rose (1987) deduced that this skeleton was indicative of a highly arboreal animal, similar to some extant procyonid and viverrid carnivorans, which was different from the locomotor mode that would have been expected for an ungulate ancestor. Rose (1990) later described more material of an indeterminate species of *Chriacus* that looked like it belonged to a more scansorial animal, but still with some arboreal capabilities. Finally, Rose (1996) described teeth and associated postcrania belonging to *Ch. truncatus* (= *Ch. baldwini*) that showed cursorial adaptations closer to early ungulates such as *Diacodexis*. This conflicting literature and the unsettled taxonomy and relationships of the numerous species of *Chriacus* suggest that either the genus *Chriacus* was highly variable in its locomotor behaviors or that the many species of *Chriacus* may not be closely related but instead belong to an array of species of varying phylogenetic position and biological attributes.

Focusing specifically on the *Ch. pelvidens* specimens we are studying, we cannot use the extremely fragmentary postcranial material associated with NMMNH P-62258 to assess locomotor behavior. Furthermore, these scrappy postcranial elements are the only postcranial bones yet recovered or recognized as belonging to *Ch. pelvidens*. Thus, we must rely on the semicircular canals of the bony labyrinth to shed light on the locomotion and agility of this species. Depending on the body mass used in the calculation of the agility score, *Ch. pelvidens* was more agile than *Ca. coarctatus* but less agile than *Protungulatum* sp. (if a high body mass estimate is used), or was as agile as *Protungulatum* sp., *H. lepidus* and *D. ilicis* (when using a low body mass estimate). The postcrania described for *Ch. baldwini* by Rose (1996) revealed that this particular species may have been cursorial, similar to artiodactyls. Extant artiodactyls of a similar body mass such as *Hydropotes inermis* (water deer) and *Tragulus javanicus* (Java mouse-deer) have an agility score of 4, which is higher than our agility score for *Ch. baldwini* of between 2 and 3 (Cox & Jeffery, 2010). Overall, while some *Chriacus* specimens or taxa may have been scansorial, cursorial or arboreal, as described above (Rose, 1990, 1996), it is unlikely that *Chriacus* was highly agile. The signal carried by the semicircular canal radius was not similar to some extant carnivorans such as viverrids (agility score 4; Spoor et al., 2007), as suggested by Rose (1987) for his uncertain species of *Chriacus*, or to artiodactyls as suggested by Rose (1996) based on those agility scores. Compared with carnivorans with an agility score of 3, *Ch. pelvidens* was more similar to *Procyon cancrivorus* (crab-eating raccoon), *Taxidea taxus* (American badger) or the lighter raccoon dog (*Nyctereutes procyonoides viverrinus*), depending on the body mass used (Spoor et al., 2007). Compared with extant mammals with an agility score of 2, *Ch. baldwini* was more similar to *Phalanger orientalis* (northern common cuscus) and *Lophiomys imhausi* (crested rat; Spoor et al., 2007). It cannot be ruled out that *Ch. pelvidens* or *Ch. baldwini* were able to climb trees based on these agility scores, because some scansorial carnivorans and marsupials have similar scores. They could also potentially have been cursorial, but to our knowledge, no modern analogue portrays this behavior with such low agility scores at a similar body mass (see Cox & Jeffery, 2010).

It is worth noting that agility scores should be interpreted with caution, as explained by Macrini et al. (2010). First, these scores require a body mass calculation, and

estimations of body mass for fossils can vary greatly when using different proxies, such as dental vs. postcranial equations (Damuth & MacFadden, 1990). Secondly, these scores were based on extant mammals that were classified into locomotor categories based on video footage of behavior (Spoor et al., 2007). However, it is unclear how representative such video footage is of the wide spectrum of locomotor abilities that species are capable of (see Macrini et al., 2010).

Implications for phylogenetic characters and character states

A close relationship between *Chriacus* and Artiodactyla has been proposed multiple times based on postcranial and dental elements from different species: *Ch. baldwini* (Van Valen, 1971, 1978), *Chriacus* sp. (Rose, 1996), and *Ch. truncatus* (= *Ch. baldwini*; Rose, 1996). However, Rose (1987) concluded that postcrania from another *Chriacus* sp. specimen – the arboreal specimen discussed above – bore little resemblance to the unequivocal early artiodactyl *Diacodexis*, and thus raised doubts about the long-considered link between the two. More recently, the numerical phylogenetic analysis of Ladevèze et al. (2010) found *Chriacus* nested within the sister-clade to Artiodactyla (including *Diacodexis*) based on specimens belonging to *Chriacus* sp. (Rose, 1987) and *Ch. orthogonius* (Szalay & Lucas, 1996). It is worth noting that in the consensus tree of the same study, *Chriacus* is placed in a polytomy with artiodactyls, perissodactyls and other archaic placentals. The phylogenetic analysis of De Bast & Smith (2013) also found *Ch. pelvidens* to be closely related to a group including *Diacodexis*. However, the resolution is also poor for this analysis and *Diacodexis* is part of a large polytomy. Perhaps surprisingly, however, Halliday et al. (2017) recovered *Chriacus* closer to carnivorans and pangolins than to artiodactyls, based on character scores from a variety of *Chriacus* specimens and species (*Ch. pelvidens*, *Ch. baldwini*, *Ch. pusillus*, *Ch. calenancus*, *Ch. katrinae* and *Ch. oconostotae*) pooled together in a composite genus-level taxon. Therefore, it is currently unclear which species of *Chriacus* may, or may not, be closely related to which extant placental orders.

Internal endocranial anatomy may help shed light on the affinities of *Chriacus*, but such morphological data have yet to be considered in comparative phylogenetic studies of the taxon. *Chriacus* shares the ancestral bony labyrinth features described in Macrini et al. (2013), with the potential stem euungulate *Protungulatum* sp. (Orliac & O'Leary, 2016), the early artiodactyl *D. ilicis* (Orliac et al., 2012b), the 'condylarth' *H. lepidus* (Ladevèze et al., 2010; Ravel & Orliac, 2015) and the 'archaic' pantodont *A. inopinata* (Muizon et al., 2015). For example, the following are all present in the above taxa: presence of the second common crus between the LSC and the PSC, the low position of the LSC plane relative to the ampulla of the PSC, and the ASC being the canal with the greatest radius and being higher than the PSC. These are all likely ancestral features for Theria (Ekdale, 2013), so this is not unexpected.

Our modified version of the Macrini et al. (2013) dataset allows us to compare explicitly the bony labyrinth features of *Chriacus* with those of other early placentals and close relatives, establish similarities with key taxa, and propose potential synapomorphies that can later be tested in a numerical phylogenetic analysis of the entire skeleton. In general, both species of *Chriacus* possess the inferred ancestral state of Placentalia for most characters in the dataset (see Macrini et al., 2013 for details of how ancestral states were estimated). The features representing potentially derived characteristics relative to the placental ancestral state relate to the anterior and lateral ampullae position (#9), the housing of the utricle and saccule (#15), the utricle chamber position (#16) and the fenestra cochleae diameter (#25). Most importantly, the dataset suggests that two bony labyrinth characters might support the affinity of both species of *Chriacus* with *D. ilicis* and/or *Protungulatum* sp., all of which are commonly held to be members or close relatives of Euungulata. First, character #15 corresponds to the utricle (elliptical recess) and saccule (spherical recess) housing. For this character, *Ch. pelvidens*, *Ch. baldwini, D. ilicis* and *Protungulatum* sp. have the utricle (elliptical recess) and saccule (spherical recess) housed within distinct, but not separated, chambers in the bony labyrinth. Secondly, character #16 relates to the position of the utricle chamber (Supporting Information Fig. S5). This structure is located closer to the anterior end of the LSC in *Ch. pelvidens*, *Ch. baldwini, D. ilicis* and *Protungulatum* sp. than in other taxa (Table 4).

We note here some additional neurosensory features, not included in our modified version of the Macrini et al. (2013) dataset, that may be phylogenetically informative and help clarify the relationships of *Ch. pelvidens*. The fenestra cochleae extends posteriorly beyond the PSC in *Ch. pelvidens*, *Protungulatum* sp., *D. ilicis* and *H. lepidus*, but not in *A. inopinata*. *Chriacus pelvidens* and *Protungulatum* sp. have a preserved cochlear fossula and aqueduct for the cochlear fossula; however, *Ch. pelvidens, D. ilicis* and *H. lepidus* do not display a horseshoe-shaped outpocketing, in contrast to *Protunguatum* sp. It is worth noting that both *D. ilicis* and *H. lepidus* exhibit a much larger fenestra cochleae compared with *Ch. pelvidens* and *Protungulatum* sp. The configuration of the fenestra cochleae in *Ch. pelvidens* could thus represent an intermediate state between more basal and derived Euungulata.

The cranial endocast of *Ch. baldwini* shares ancestral features with other early placental mammals related to the relative sizes of the brain, olfactory bulb and petrosal lobule. They all have a relatively low EQ, below 0.50, which has been considered the minimum value for extant mammals (Rowe et al., 2011; Hoffmann et al., 2014; see discussion in

Cameron et al., 2019). The olfactory bulbs represent more than 6% of total brain volume, which has been considered the ancestral state for the common ancestor of therians by Macrini et al. (2007, character 1). *Diacodexis ilicis* and *H. lepidus* as well as many Eocene artiodactyls also bear the same ancestral condition for the olfactory bulbs (Orliac & Gilissen, 2012). The petrosal lobules of *Ch. baldwini, D. ilicis* and *H. lepidus* represent less than 1% of brain volume (Ch. #15), which is the ancestral condition for therians and is also found in some Mesozoic mammals (*Vincelestes* and *Hadrocodium*; paraflocculi in Macrini, 2006).

Conclusions

Reconstructions of the bony labyrinth and cranial endocasts of *Ch. pelvidens* and *Ch. baldwini* shed light on the neurosensory systems and help illuminate the biology and behaviors of Paleocene 'archaic' placental mammals. *Chriacus baldwini* probably relied heavily on its sense of smell as other early placental mammals such as *Ca. coarctatus* (Cameron et al., 2019) and *O. tisonensis* (Napoli et al., 2018), but less so on vision (including a low vestibulo-ocular reflex) because its petrosal lobules and neocortex were not as developed as in mammals with enhanced eyesight, such as squirrels (Bertrand et al., 2017). *Chriacus pelvidens* and *Ch. baldwini* were probably slow- to medium-moving mammals based on semicircular canal data, and *Ch. pelvidens* was able to hear a range of sounds that may have been similar to that of the extant aardvark and nine-banded armadillo. The bony labyrinth provides new data supporting the potential relationship between *Ch. pelvidens, Ch. baldwini* and extant placental mammals. *Chriacus* shares derived features in the vestibular region with the early artiodactyl *Diacodexis* and some potential Paleogene stem Euungulata, particularly in the housing of the utricle and saccule (elliptical and spherical recesses). The bony labyrinth morphology may partly support other studies (e.g. Van Valen, 1978; Rose, 1996; Ladevèze et al., 2010; De Bast & Smith, 2013), which have hypothesized that *Chriacus* is closely related to Euungulata, and perhaps Artiodactyla, based on either non-numerical phylogenetic reasoning or highly homoplastic and poorly resolved phylogenetic analyses. This result also shows the potential of using bony labyrinth morphology to improve our understanding of the phylogenetic relationships between early and modern placental mammals.

Acknowledgements

We thank U. Denetclaw for assistance in the field and M. J. Orliac and the AMNH for providing access to the CT scans and 3D models of the bony labyrinth and cranial endocasts of *Protungulatum*, *Diacodexis* and *Hyopsodus*. We would like to thank M. J. Orliac and an anonymous reviewer for helpful comments that improved this manuscript. This research was funded by a Marie Skłodowska-Curie Actions: Individual Fellowship (H2020-MSCA-IF-2018-2020; No. 792611) to O.C.B.; a European Research Council (ERC) Starting Grant (No. 756226) to S.L.B., under the European Union's Horizon 2020 Research and Innovation Programme; and the National Science Foundation (DEB: 1654949) to J.R.W., (EAR: 1325544 and DEB: 1654952) to S.L.B. and T.E.W., and (DEB: 1456826) to L.T.H. and S.G.B.C. There is no conflict of interest.

Author contributions

O.C.B. and S.L.B. conceived and designed the study. I.B.B., L.T.H. and S.G.B.C. acquired the CT data. T.E.W. provided CT data and dental measurements. O.C.B. did all segmentations and drafted the manuscript, tables and figures. Analyses and interpretations were performed by O.C.B. and critically reviewed by S.L.B., S.L.S., J.R.W., T.E.W., L.T.H. and S.G.B.C. All authors revised the manuscript and provided final approval before submission.

Data availability statement

The surface renderings of the cranial and bony labyrinth endocasts described in this paper are available in MorphoSource (www.morphosource.org; Boyer et al. 2014) at http://morphosource.org/Detail/ProjectDetail/Show/project_id/830

References

Alroy J (1999) The fossil record of North American mammals: evidence for a Paleocene evolutionary radiation. *Syst Biol* **48**, 107–118.

Ameghino F (1901) Notices préliminaires sur des ongulés nouveaux des terrains crétacés de Patagonie. *Bol Acad Nac Cienc* **16**, 349–426.

Archibald JD (1998) Archaic ungulates ('Condylarthra'). In: *Evolution of Tertiary Mammals of North America, Volume 1, Terrestrial Carnivores, Ungulates, and Ungulate-Like Mammals*. (eds Janis CM, Scott KM, Jacobs LL), pp. 292–331. Cambridge: Cambridge University Press.

Axelsson A, Ryan AF (1988) Circulation of the inner ear: I. Comparative study of the vascular anatomy in the mammalian cochlea. In: *Physiology of the Ear*. (eds Jahn AF, Santos-Sacchi J), pp. 295–316. San Diego: Singular Publishing.

Bast ED, Smith T (2013) Reassessment of the small 'arctocyonid' *Prolatidens waudruae* from the early Paleocene of Belgium, and its phylogenetic relationships with ungulate-like mammals. *J Vertebr Paleontol* **33**, 964–976.

Bertrand OC, Amador-Mughal F, Silcox MT (2016) Virtual endocasts of Eocene *Paramys* (Paramyinae): oldest endocranial record for Rodentia and early brain evolution in Euarchontoglires. *Proc R Soc B* **283**, 1–8.

Bertrand OC, Amador-Mughal F, Silcox MT (2017) Virtual endocast of the early Oligocene *Cedromus wilsoni* (Cedromurinae) and brain evolution in squirrels. *J Anat* **230**, 128–151.

Bertrand OC, Amador-Mughal F, Lang MM, et al. (2018a) New virtual endocasts of Eocene Ischyromyidae and their relevance in evaluating neurological changes occurring through time in

Rodentia. *J Mammal Evol* **26**, 345–371.https://doi.org/10.1007/s10914-017-9425-6.

Bertrand OC, Amador-Mughal F, Lang MM, et al. (2018b) Virtual endocasts of fossil Sciuroidea: brain size reduction in the evolution of fossoriality. *Palaeontology* **61**, 919–948.

Billet G, Bardin J (2018) Serial homology and correlated characters in morphological phylogenetics: modeling the evolution of dental crests in placentals. *Syst Biol* **68**, 267–280.

Billet G, Muizon C de (2013) External and internal anatomy of a petrosal from the late Paleocene of Itaboraí, Brazil, referred to Notoungulata (Placentalia). *J Vertebr Paleontol* **33**, 455–469.

Billet G, Muizon C de, Schellhorn R, et al. (2015) Petrosal and inner ear anatomy and allometry amongst specimens referred to Litopterna (Placentalia). *Zool J Linn Soc* **173**, 956–987.

Bloch JI, Silcox MT, Boyer DM, et al. (2007) New Paleocene skeletons and the relationship of plesiadapiforms to crown-clade primates. *Proc Natl Acad Sci* **104**, 1159–1164.

Boyer DM, Kaufman S, Gunnell GF, et al. (2014) Managing 3D digital data sets of morphology: MorphoSource is a new project-based data archiving and distribution tool. *Am J Phys Anthropol* **153**(Suppl 58), 84.

Burgin CJ, Colella JP, Kahn PL, et al. (2018) How many species of mammals are there? *J Mammal* **99**, 1–14.

Cameron J, Shelley SL, Williamson TE, et al. (2019) The brain and inner ear of the early Paleocene 'condylarth' *Carsioptychus coarctatus*: implications for early placental mammal neurosensory biology and behavior. *Anat Rec* **302**, 306–324.

Carrano MT (1999) What, if anything, is a cursor? Categories versus continua for determining locomotor habit in mammals and dinosaurs. *J Zool* **247**, 29–42.

Chester SGB, Williamson TE, Bloch JI, et al. (2017) Oldest skeleton of a plesiadapiform provides additional evidence for an exclusively arboreal radiation of stem primates in the Palaeocene. *R Soc Open Sci* **4**, 1–9.

Cifelli RL (1983) The origin and affinities of the South American Condylarthra and early Tertiary Litopterna (Mammalia). *Am Mus Novit* **2772**, 1–49.

Collinson ME, Hooker JJ (1987) Vegetational and mammalian faunal changes in the Early Tertiary of southern England. In: *The Origins of Angiosperms and Their Biological Consequences*. (eds Friis EM, Chaloner WG, Crane PR), pp. 259–304. Cambridge: Cambridge University Press.

Cope ED (1875) Systematic catalogue of Vertebrata of the Eocene of New Mexico by parties of the expedition of 1874, Chapter 12: Fossils of the Eocene period. Geographical Surveys West of the 100th Meridian, G. M. Wheeler, Corps of Engineers, U.S. Army, Washington, DC 4, 37–282.

Cope ED (1881a) Geology and palaeontology – a new type of Perissodactyla. *Am Nat* **15**, 1017–1018.

Cope ED (1881b) Geology and palaeontology – notes on Creodonta. *Am Nat* **15**, 1018–1019.

Cope ED (1882) Synopsis of the Vertebrata of the Puerco Eocene epoch. *Proc Am Philos Soc* **20**, 461–471.

Cope ED (1884a) The Condylarthra. *Am Nat* **18**, 790–805.

Cope ED (1884b) The Condylarthra (continued). *Am Nat* **18**, 892–906.

Cox PG, Jeffery N (2010) Semicircular canals and agility: the influence of size and shape measures. *J Anat* **216**, 37–47.

Damuth J (1990) Problems in estimating body masses of archaic ungulates using dental measurements. In: *Body Size in Mammalian Paleobiology: Estimation and Biological Implications*. (eds Damuth J, MacFadden BJ), pp. 229–253. Cambridge: Cambridge University Press.

Damuth J, MacFadden BJ (eds.) (1990) *Body Size in Mammalian Paleobiology: Estimation and Biological Implications*. New York: Cambridge University Press.

dos Reis M, Inoue J, Hasegawa M, et al. (2012) Phylogenomic datasets provide both precision and accuracy in estimating the timescale of placental mammal phylogeny. *Proc R Soc B* **279**, 3491–3500.

dos Reis M, Donoghue PC, Yang Z (2014) Neither phylogenomic nor palaeontological data support a Palaeogene origin of placental mammals. *Biol Lett* **10**, 1–4.

Edinger T (1964) Midbrain exposure and overlap in mammals. *Am Zool* **4**, 5–19.

Eisenberg JF (1981) *The Mammalian Radiations: An Analysis of Trends in Evolution, Adaptation, and Behavior*. Chicago: University of Chicago Press.

Ekdale EG (2009) Variation within the bony labyrinth of mammals. Ph.D. Dissertation. The University of Texas at Austin.

Ekdale EG (2013) Comparative anatomy of the bony labyrinth (inner ear) of placental mammals. *PLoS ONE* **10**, 1–100.

Ekdale EG (2016) Form and function of the mammalian inner ear. *J Anat* **228**, 324–337.

Ekdale EG, Rowe T (2011) Morphology and variation within the bony labyrinth of zhelestids (Mammalia, Eutheria) and other therian mammals. *J Vertebr Paleontol* **31**, 658–675.

Ferreira-Cardoso S, Araújo R, Martins NE, et al. (2017) Floccular fossa size is not a reliable proxy of ecology and behaviour in vertebrates. *Sci Rep* **7**, 1–11.

Gannon PJ, Eden AR, Laitman JT (1988) The subarcuate fossa and cerebellum of extant primates: comparative study of a skull-brain interface. *Am J Phy Anthropol* **77**, 143–164.

Gazin CL (1969) A new occurrence of Paleocene mammals in the Evanston Formation, southwestern Wyoming. *Smithson Contrib Paleobiol* **2**, 1–19.https://doi.org/10.5479/si.00810266.2.1

Geisler JH, Luo Z (1996) The petrosal and inner ear of *Herpetocetus* sp. (Mammalia: Cetacea) and their implications for the phylogeny and hearing of archaic mysticetes. *J Paleontol* **70**, 1045–1066.

Gingerich PD, Gunnell GF (2005) Brain of *Plesiadapis cookei* (Mammalia, Proprimates): surface morphology and encephalization compared with those of Primates and Dermoptera. *Contrib Mus Paleontol Univ Mich* **31**, 185–195.

Gray AA (1907) *The Labyrinth of Animals: Including Mammals, Birds, Reptiles and Amphibians Volume 1*. London: Churchill.

Gray H (1918) *Henry Gray's Anatomy of the Human Body*. Philadelphia: Lea and Febiger.

Grossnickle DM, Newham E (2016) Therian mammals experience an ecomorphological radiation during the Late Cretaceous and selective extinction at the K-Pg boundary. *Proc R Soc B* **283**, 1–8.

Halliday TJD, Goswami A (2016a) Eutherian morphological disparity across the end-Cretaceous mass extinction. *Biol J Linn Soc* **118**, 152–168.

Halliday TJD, Goswami A (2016b) The impact of phylogenetic dating method on interpreting trait evolution: a case study of Cretaceous-Palaeogene eutherian body-size evolution. *Biol Lett* **12**, 1–5.

Halliday TJD, Upchurch P, Goswami A (2016) Eutherians experienced elevated evolutionary rates in the immediate aftermath of the Cretaceous-Palaeogene mass extinction. *Proc R Soc B* **283**, 1–8.

Halliday TJ, Upchurch P, Goswami A (2017) Resolving the relationships of Paleocene placental mammals. *Biol Rev* **92**, 521–550.

Hiramatsu T, Ohki M, Kitazawa H, et al. (2008) Role of primate cerebellar lobulus petrosus of paraflocculus in smooth pursuit eye movement control revealed by chemical lesion. *Neurosci Res* **60**, 250–258.

Hoffmann S, O'Connor PM, Kirk EC, et al. (2014) Endocranial and inner ear morphology of *Vintana sertichi* (Mammalia, Gondwanatheria) from the Late Cretaceous of Madagascar. *J Vertebr Paleontol Mem* **34**, 110–137.

Hooker JJ, Collinson ME (2012) Mammalian faunal turnover across the Paleocene-Eocene boundary in NW Europe: the roles of displacement, community evolution and environment. *Aust J Earth Sci* **105**, 17–28.

Jerison HJ (1973) *Evolution of the Brain and Intelligence*. New York: Academic Press.

Jerison HJ (2012) Digitized fossil brains: neocorticalization. *Biol Ther Dent* **6**, 383–392.

Kangas AT, Evans AR, Thesleff I, et al. (2004) Nonindependence of mammalian dental characters. *Nature* **432**, 211–214.

Kassai Y, Munne P, Hotta Y, et al. (2005) Regulation of mammalian tooth cusp patterning by ectodin. *Science* **309**, 2067–2070.

Kielan-Jaworowska Z (1984) Evolution of the therian mammals in the Late Cretaceous of Asia. Part VI. Endocranial casts of eutherian mammals. *Palaeontol Pol* **46**, 157–171.

Kondrashov PE, Lucas SG (2004a) *Arctocyon* (Mammalia, Arctocyonidae) from the Paleocene of North America. *Bull New Mex Mus Nat Hist Sci* **26**, 11–20.

Kondrashov PE, Lucas SG (2004b) *Oxyclaenus* from the early Paleocene of New Mexico and the status of the Oxyclaeninae (Mammalia, Arctocyonidae). *Bull New Mex Mus Nat Hist Sci* **26**, 21–31.

Kondrashov PE, Lucas SG (2015) Paleocene vertebrate faunas of the San Juan Basin, New Mexico. *Bull New Mex Mus Nat Hist Sci* **68**, 131–148.

Krause DW, Gingerich PD (1983) Mammalian fauna from Douglass Quarry, earliest Tiffanian (late Paleocene) of the eastern Crazy Mountain Basin, Montana. *Contrib Mus Paleontol Univ Mich* **26**, 157–196.

Kretzoi M (1943) *Kochictis centennii* n. g. n sp., ein altertümlicher Creodonte aus dem Oberoligozän Siebenbürgens. *Földt Közl* **73**, 190–195.

Ladevèze S, Missiaen P, Smith T (2010) First skull of *Orthaspidotherium edwardsi* (Mammalia', Condylarthra') from the late Paleocene of Berru (France) and phylogenetic affinities of the enigmatic European family Pleuraspidotheriidae. *J Vertebr Paleontol* **30**, 1559–1578.

Leslie C, Peppe D, Williamson T, et al. (2018) High-resolution magnetostratigraphy of the Upper Nacimiento Formation, San Juan Basin, New Mexico, USA: implications for basin evolution and mammalian turnover. *Am J Sci* **318**, 300–334.

Legendre S (1989) Les communautés de mammifères du Paléogène (Eocène supérieur et Oligocène) d'Europe occidentale: structures, milieux et évolution. *Münchner Geowiss Abhand A Geol Paläontol* **16**, 1–110.

Liu L, Zhang J, Rheindt FE, et al. (2017) Genomic evidence reveals a radiation of placental mammals uninterrupted by the KPg boundary. *Proc Natl Acad Sci U S A* **114**, e7282–E7290.

Long A, Bloch JI, Silcox MT (2015) Quantification of neocortical ratios in stem primates. *Am J Phys Anthropol* **157**, 363–373.

Luo ZX (2007) Transformation and diversification in early mammal evolution. *Nature* **450**, 1011–1019.

Luo Z, Eastman ER (1995) Petrosal and inner ear of a squalodontoid whale: implications for evolution of hearing in odontocetes. *J Vertebr Paleontol* **15**, 431–442.

Luo Z, Marsh K (1996) Petrosal (periotic) and inner ear of a Pliocene kogiine whale (Kogiinae, Odontoceti): implications on relationships and hearing evolution of toothed whales. *J Vertebr Paleontol* **16**, 328–348.

MacPhee RD (1981) Auditory regions of primates and eutherian insectivores. *Contrib Primatol* **18**, 1–282.

Macrini TE (2006) The evolution of endocranial space in mammals and non-mammalian cynodonts. Ph.D. dissertation. The University of Texas at Austin.

Macrini TE, Rougier GW, Rowe T (2007) Description of a cranial endocast from the fossil mammal *Vincelestes neuquenianus* (Theriiformes) and its relevance to the evolution of endocranial characters in therians. *Anat Rec* **290**, 875–892.

Macrini TE, Flynn JJ, Croft DA, et al. (2010) Inner ear of a notoungulate placental mammal: anatomical description and examination of potentially phylogenetically informative characters. *J Anat* **216**, 600–610.

Macrini TE, Flynn JJ, Ni X, et al. (2013) Comparative study of notoungulate (Placentalia, Mammalia) bony labyrinths and new phylogenetically informative inner ear characters. *J Anat* **223**, 442–461.

Malinzak MD, Kay RF, Hullar TE (2012) Locomotor head movements and semicircular canal morphology in primates. *Proc Natl Acad Sci U SA* **109**, 17914–17919.

Martin RD (1990) *Primate Origins and Evolution: A Phylogenetic Reconstruction*. London: Chapman and Hall.

Matthew WD (1897) A revision of the Puerco Fauna. *Bull Am Mus Nat Hist* **9**, 259–323.

Matthew WD (1915) A review of the lower Eocene Wasatch and Wind River faunas. Part I. —Order Ferae (Carnivora). Suborder Creodonta. *Bull Am Mus Nat Hist* **34**, 1–103.

Matthew WD (1937) Paleocene faunas of the San Juan Basin, New Mexico. *Trans Am Philos Soc* **30**, 1–510.

McClure TD, Daron GH (1971) The relationship of the developing inner ear, subarcuate fossa and paraflocculus in the rat. *Am J Anat* **130**, 235–249.

Meng J, Fox RC (1995) Osseous inner ear structures and hearing in early marsupials and placentals. *Zool J Linn Soc* **115**, 47–71.

Mennecart B, Costeur L (2016) Shape variation and ontogeny of the ruminant bony labyrinth, an example in Tragulidae. *J Anat* **229**, 422–435.

Muizon C de, Billet G, Argot C, et al. (2015) *Alcidedorbignya inopinata*, a basal pantodont (Placentalia, Mammalia) from the early Palaeocene of Bolivia: anatomy, phylogeny and palaeobiology. *Geodiversitas* **37**, 397–634.

Muller M (1994) Semicircular duct dimensions and sensitivity of the vertebrate vestibular system. *J Theor Biol* **167**, 239–256.

Murphy WJ, Eizirik E, Johnson WE, et al. (2001) Molecular phylogenetics and the origins of placental mammals. *Nature* **409**, 614–618.

Napoli JG, Williamson TE, Shelley SL, et al. (2018) A digital endocranial cast of the early Paleocene (Puercan) 'archaic' mammal *Onychodectes tisonensis* (Eutheria: Taeniodonta). *J Mammal Evol* **25**, 179–195.

Novacek MJ (1986) The skull of leptictid insectivorans and the higher-level classification of eutherian mammals. *Bull Am Mus Nat Hist* **183**, 1–112.

Nowak RM (1999) *Walker's Mammals of the World*. Baltimore: Johns Hopkins University press.

O'Leary MA, Bloch JI, Flynn JJ, et al. (2013) The placental mammal ancestor and the post–K-Pg radiation of placentals. *Science* **339**, 662–667.

Oman CM, Marcus EN, Curthoys IS (1987) The influence of semicircular canal morphology on endolymph flow dynamics: an anatomically descriptive mathematical model. *Acta Oto-Laryngol* **103**, 1–13.

Orliac MJ, Gilissen E (2012) Virtual endocranial cast of earliest Eocene *Diacodexis* (Artiodactyla, Mammalia) and morphological diversity of early artiodactyl brains. *Proc R Soc B* **279**, 3670–3677.

Orliac MJ, O'Leary MA (2016) The inner ear of *Protungulatum* (pan-Euungulata, Mammalia). *J Mammal Evol* **23**, 337–352.

Orliac MJ, Argot C, Gilissen E (2012a) Digital cranial endocast of *Hyopsodus* (Mammalia', Condylarthra'): a case of Paleogene terrestrial echolocation? *PLoS ONE* **7**, 1–10.

Orliac MJ, Benoit J, O'Leary MA (2012b) The inner ear of *Diacodexis*, the oldest artiodactyl mammal. *J Anat* **221**, 417–426.

Orliac MJ, Ladevèze S, Gingerich PD, et al. (2014) Endocranial morphology of Palaeocene *Plesiadapis tricuspidens* and evolution of the early primate brain. *Proc R Soc B* **281**, 1–7.

Orliac MJ, Araújo R, Lihoreau F (2017) The petrosal and bony labyrinth of *Diplobune minor*, an enigmatic Artiodactyla from the Oligocene of Western Europe. *J Morphol* **278**, 1168–1184.

Osborn HF, Earle C (1895) Fossil mammals of the Puerco beds: collection of 1892. *Bull Am Mus Nat Hist* **7**, 1–71.

Paleobiology Database (2019) Group name 'Eutheria', time intervals = 66-56 Ma. Accessed 4 May 2019. https://paleobiodb.org/classic/displayDownloadGenerator

Patterson B, McGrew PO (1962) A new arctocyonid from the Paleocene of Wyoming. *Breviora* **174**, 1–10.

Penkrot TA (2010) Molar morphometrics and diet in North American condylarths. Ph.D. Thesis, Baltimore: Johns Hopkins University.

Prothero DR, Manning EM, Fischer M (1988) The phylogeny of the ungulates. In: *The Phylogeny and Classification of the Tetrapods. Volume 2: Mammals* (ed. Benton MJ), pp. 201–234. Oxford: Clarendon Press.

Radinsky L (1977) Brains of early carnivores. *Paleobiology* **3**, 333–349.

Rambold H, Churchland A, Selig Y, et al. (2002) Partial ablations of the flocculus and ventral paraflocculus in monkeys cause linked deficits in smooth pursuit eye movements and adaptive modification of the VOR. *J Neurophysiol* **87**, 912–924.

Ravel A, Orliac MJ (2015) The inner ear morphology of the 'condylarthran' *Hyopsodus lepidus*. *Hist Biol* **27**, 957–969.

Rose KD (1987) Climbing adaptations in the early Eocene mammal *Chriacus* and the origin of Artiodactyla. *Science* **236**, 314–316.

Rose KD (1990) Postcranial skeletal remains and adaptations in early Eocene mammals from the Willwood Formation, Bighorn Basin, Wyoming. *Geol Soc Am Spec Pap* **243**, 107–133.

Rose KD (1996) On the origin of the order Artiodactyla. *Proc Natl Acad Sci US A* **93**, 1705–1709.

Rose KD (2006) *The Beginning of the Age of Mammals*. Baltimore: Johns Hopkins University Press.

Rosowski JJ (1992) Hearing in transitional mammals: predictions from the middle-ear anatomy and hearing capabilities of extant mammals. In: *The Evolutionary Biology of Hearing*. (eds Webster DB, Fay RR, Popper AN), pp. 615–631. New York: Springer-Verlag.

Rosowski JJ, Graybeal A (1991) What did *Morganucodon* hear? *Zool J Linn Soc* **101**, 131–168.

Rougier GW, Wible JR, Novacek MJ (1998) Implications of *Deltatheridium* specimens for early marsupial history. *Nature* **396**, 459–463.

Rowe T (1996) Coevolution of the mammalian middle ear and neocortex. *Science* **273**, 651–654.

Rowe TB, Macrini TE, Luo ZX (2011) Fossil evidence on origin of the mammalian brain. *Science* **332**, 955–957.

Russell DE (1964) Les mammifères paléocènes d'Europe. *Mém Mus Natl Hist Nat Sér C* **13**, 1–324.

Russell DE, Zhai R (1987) The Paleogene of Asia: mammals and stratigraphy. *Mém Mus Natl Hist Nat Sér C* **52**, 1–488.

Sakamoto A, Kuroda Y, Kanzaki S, et al. (2017) Dissection of the auditory bulla in postnatal mice: isolation of the middle ear bones and histological analysis. *J Vis Exp* **119**, e55054.

Sansom RS, Wills MA, Williams T (2017) Dental data perform relatively poorly in reconstructing mammal phylogenies: morphological partitions evaluated with molecular benchmarks. *Syst Biol* **66**, 813–822.

Schmelzle T, Sánchez-Villagra MR, Maier W (2007) Vestibular labyrinth diversity in diprotodontian marsupial mammals. *Mammal Study* **32**, 83–97.

Schwarz DWF, Tomlinson RD (1994) Physiology of the vestibular system. In: *Neurotology*. (eds Jackler RK, Brackmann DE), pp. 59–98. St. Louis: Mosby.

Segall W (1970) Morphological parallelisms of the bulla and auditory ossicles in some insectivores and marsupials. *Field Zool* **51**, 169–205.

Silcox MT, Bloch JI, Boyer DM, et al. (2009a) Semicircular canal system in early primates. *J Hum Evol* **56**, 315–327.

Silcox MT, Dalmyn CK, Bloch JI (2009b) Virtual endocast of *Ignacius graybullianus* (Paromomyidae, Primates) and brain evolution in early primates. *Proc Natl Acad Sci U S A* **106**, 10987–10992.

Silcox MT, Benham AE, Bloch JI (2010) Endocasts of *Microsyops* (Microsyopidae, Primates) and the evolution of the brain in primitive primates. *J Hum Evol* **58**, 505–521.

Silcox MT, Dalmyn CK, Hrenchuk A, et al. (2011) Endocranial morphology of *Labidolemur kayi* (Apatemyidae, Apatotheria) and its relevance to the study of brain evolution in Euarchontoglires. *J Vertebr Paleontol* **31**, 1314–1325.

Simpson GG (1945) The principles of classification and a classification of mammals. *Bull Am Mus Nat Hist* **85**, 1–350.

Slater GJ (2013) Phylogenetic evidence for a shift in the mode of mammalian body size evolution at the Cretaceous-Palaeogene boundary. *Methods Ecol Evol* **4**, 734–744.

Spoor F, Zonneveld F (1998) Comparative review of the human bony labyrinth. *Am J Phys Anthropol* **107**, 211–251.

Spoor F, Garland T Jr., Krovitz G, et al. (2007) The primate semicircular canal system and locomotion. *Proc Natl Acad Sci U S A* **104**, 10808–10812.

Szalay FS, Lucas SG (1996) The postcranial morphology of paleocene *Chriacus* and *Mixodectes* and the phylogenetic relationships of archontan mammals. *Bull New Mex Mus Nat Hist Sci* **7**, 1–47.

Van Valen L (1966) Deltatheridia, a new order of mammals. *Bull Am Mus Nat Hist* **132**, 1–126.

Van Valen L (1971) Toward the origin of artiodactyls. *Evolution* **25**, 523–529.

Van Valen L (1978) The beginning of the age of mammals. *Evol Theory* **4**, 45–80.

Visualization Sciences Group (1995–2018) *Avizo®9.0.1 Konrad-Zuse-Zentrum für Informationstechnik*. Berlin: Berlin (ZIB).

West CD (1985) The relationship of the spiral turns of the cochlea and the length of the basilar membrane to the range

of audible frequencies in ground dwelling mammals. *J Acoust Soc Am* **77**, 1091–1101.

Wible JR (2008) On the cranial osteology of the Hispaniolan solenodon, *Solenodon paradoxus* Brandt, 1833 (Mammalia, Lipotyphla, Solenodontidae). *Ann Carnegie Mus* **77**, 321–402.

Wible JR (2010) Petrosal anatomy of the nine-banded armadillo, *Dasypus novemcinctus* Linnaeus, 1758 (Mammalia, Xenarthra, Dasypodidae). *Ann Carnegie Mus* **79**, 1–29.

Wible JR, Rougier GW, Novacek MJ, et al. (2007) Cretaceous eutherians and Laurasian origin for placental mammals near the K/T boundary. *Nature* **447**, 1003–1006.

Wible JR, Rougier GW, Novacek MJ, et al. (2009) The eutherian mammal *Maelestes gobiensis* from the Late Cretaceous of Mongolia and the phylogeny of Cretaceous Eutheria. *Bull Am Mus Nat Hist* **327**, 1–123.

Williamson TE (1996) The beginning of the Age of Mammals in the San Juan Basin, New Mexico: biostratigraphy and evolution of Paleocene mammals of the Nacimiento Formation. *Bull New Mex Mus Nat Hist Sci* **8**, 1–141.

Williamson TE, Carr TD (2007) Revision of the problematic early Paleocene genus *Oxyclaenus* (Mammalia: Oxyclaenidae) and a new species of *Carcinodon*. *J Vertebr Paleontol* **27**, 973–986.

Williamson TE, Lucas SG (1993) Paleocene vertebrate paleontology of the San Juan Basin, New Mexico. *Bull New Mex Mus Nat Hist Sci* **2**, 105–135.

Wilson GP (2013) Mammals across the K/Pg boundary in northeastern Montana, USA: dental morphology and body-size patterns reveal extinction selectivity and immigrant-fueled ecospace filling. *Paleobiology* **39**, 429–469.

Zou Z, Zhang J (2016) Morphological and molecular convergences in mammalian phylogenetics. *Nat Commun* **7**, 1–9.

Supporting Information

Additional Supporting Information may be found in the online version of this article: